

RI 9062

RI	9062
-----------	-------------

PLEASE DO NOT REMOVE FROM LIBRARY

Bureau of Mines Report of Investigations/1987

Coal Mine Hazard Detection Using In-Seam Ground-Penetrating-Radar Transillumination

By Maureen M. Foss and Richard J. Leckenby



UNITED STATES DEPARTMENT OF THE INTERIOR

Report of Investigations 9062

Coal Mine Hazard Detection Using In-Seam Ground-Penetrating-Radar Transillumination

By Maureen M. Foss and Richard J. Leckenby



UNITED STATES DEPARTMENT OF THE INTERIOR
Donald Paul Hodel, Secretary

BUREAU OF MINES
Robert C. Horton, Director

Library of Congress Cataloging in Publication Data:

Foss, Maureen M

Coal mine hazard detection using in-seam ground-penetrating-radar
transillumination.

(Report of investigations ; 9062)

Bibliography: p. 26.

Supt. of Docs. no.: I 28.23: 9062.

1. Coal mines and mining—Safety measures. 2. Ground penetrating radar. I. Lecken-
by, Richard J. II. Title. III. Series: Report of investigations (United States. Bureau of
Mines) ; 9062

TN23.U43

[TN295]

622 s [622'.8]

86-600286

CONTENTS

	<u>Page</u>
Abstract.....	1
Introduction.....	2
Acknowledgments.....	4
Evaluation of probable accuracy.....	4
Air tests.....	4
Air test 1: Normal moveout.....	5
Air test 2: Parallel moveout.....	7
Air test 3: Circular test.....	8
Air test 4: Receiver rotation.....	9
Coal tests.....	10
Coal test 1: Rotation of receiver antenna.....	10
Coal tests 2 and 3: Moveout parallel to coal rib.....	11
Evaluation conclusions.....	14
Detectability.....	15
Velocity radar tomography.....	16
Phase 1: Data acquisition.....	17
Phase 2: Velocity tomography.....	17
Implementation.....	17
Results.....	20
Phase 3: Clay vein model.....	24
Conclusions and recommendations.....	25
References.....	26
Appendix.....	27

ILLUSTRATIONS

1. Model transillumination configuration.....	3
2. Antennas and easels used for the air tests.....	5
3. Air test grid.....	5
4. Computer plot of recorded waves from air test 1.....	6
5. Air test 1, measured time versus distance and best fitted curve.....	7
6. Air test 1, measured amplitude data and best fitted curve.....	7
7. Air test 2, measured time versus distance and best fitted curve.....	8
8. Air test 2, measured amplitude data and best fitted curve.....	9
9. Plan view of coal mine test pillar.....	10
10. Coal test 1, rotation of receiver antenna; computer plot of the recorded waves ranging from 0° rotation on the left to 90° rotation on the right..	11
11. Coal test 1, rotation of receiver antenna; plot of amplitude versus receiver rotational angle.....	12
12. Coal test 2, moveout parallel to coal rib.....	12
13. Coal tests 2 and 3, measured time versus distance and best fitted curves..	13
14. Coal tests 2 and 3, measured amplitude versus distance and best fitted curves.....	14
15. Plan view of coal pillar design used for detectability modeling.....	15
16. Plot of model time ratio versus width ratio for different velocity ratios.	16
17. Plot of model amplitude ratio versus width ratio for different attenuation ratios.....	16
18. Plan view of Bruceton Coal Research Mine test pillar containing a clay vein.....	17
19. Computer plot of short-pulse waveforms in order they were taken for the tomography scan.....	18

ILLUSTRATIONS--Continued

	<u>Page</u>
20. Computer plot of synthetic-pulse waves in order they were recorded.....	19
21. Representative tomographic pillar divided into 1-m-square cells or zones..	21
22. Line printer tomographic plot of velocity cells from short-pulse data.....	22
23. Gray scale tomographic plot of short-pulse data.....	22
24. Line printer tomographic plot of velocity cells from clay vein model.....	23
25. Gray scale tomographic plot of synthetic-pulse data.....	23
26. Line printer tomographic plot of velocity cells from clay vein model.....	24
27. Gray scale tomographic plot of clay vein model.....	25
A-1. Block diagram of the short-pulse system used during this investigation....	27

TABLES

1. Air test 1: Normal moveout in air.....	6
2. Air test 2: Parallel moveout test.....	8
3. Air test 3: Circular air test.....	9
4. Air test 4: Antenna rotational test.....	9
5. Coal test 1: Antenna rotational test.....	10
6. Coal test 2: Moveout test 1.....	13
7. Coal test 3: Moveout test 2.....	14

UNIT OF MEASURE ABBREVIATIONS USED IN THIS REPORT

cm	centimeter	m/s	meter per second
dB	decibel	mV	millivolt
deg	degree	ns	nanosecond
ft	foot	Ω	ohm
m	meter	%	percent
MHz	megahertz	V	volt

COAL MINE HAZARD DETECTION USING IN-SEAM GROUND-PENETRATING-RADAR TRANSILLUMINATION

By Maureen M. Foss¹ and Richard J. Leckenby²

ABSTRACT

Underground coal mining is hazardous due to changing geological conditions. One geophysical method showing promise for in-seam hazard detection is ground-penetrating radar (GPR). The Bureau of Mines recently completed preliminary studies to demonstrate the feasibility of using GPR for in-seam hazard detection. Investigations included air and coal tests for the purpose of checking equipment accuracy, coal penetration, and other factors such as the effects of receiver orientation. Further investigations involved using both a short pulse and a new prototype synthetic-pulse system to locate a clay vein in a coal seam using transillumination. Data were gathered on multiple travel paths, and a back projection processing technique was then used to create a tomographic image using the calculated velocities. A computer model of the same coal seam was subsequently processed using the same tomographic technique, and the results were compared with those of the actual data. Analysis of the tomographic images shows the presence of the clay vein, although its boundaries are unclear due to the tomography method used. Results of these preliminary studies show that GPR is feasible for use in in-seam hazard detection and point the direction that future research should take. A need has been shown for research involving more sophisticated tomography techniques, transmission studies on thicker coal seams, and reflection studies using the synthetic-pulse system.

¹Geophysical engineer.

²Physicist (now with Martin Marietta Corp., Denver, CO).
Denver Research Center, Bureau of Mines, Denver CO.

INTRODUCTION

Underground coal mining is a hazardous occupation. One reason it is so hazardous is the occurrence of unknown and unexpected changes in geological conditions. These geological conditions include clay veins, faults, sand channels, well casings, and gas or air pockets. The hazards they present include poor roof conditions, methane and water traps, and sparking sources. It is clear that advance knowledge of these hazards within the seam could save lives and improve efficiency. A number of geophysical methods have been tested and are now being used for in-seam hazard detection. One method showing great promise for near-face exploration is ground-penetrating radar, GPR (11).³

The Bureau of Mines has completed the preliminary groundwork necessary to determine the feasibility of using GPR for coal mine hazard detection. From tests the Bureau had conducted in 1970 (3) to the present, technology has slowly and steadily advanced. Recent testing was completed at the Denver Research Center, the Deseret Mine near Price, UT, and the Coal Research Mine in Bruceton, PA. The Bureau also recently completed a cost-sharing contract with XADAR Corp. (7-8) for the development of a new prototype radar system known as synthetic pulse radar. Preliminary transillumination testing performed by XADAR showed the system easily penetrating 170 ft of coal, with indications that at least 300-ft penetration is possible (7).

This increase in penetration makes transillumination and imaging techniques such as tomography feasible and practical for use in a coal seam. Figure 1 demonstrates a model of a transillumination configuration. For in-seam transillumination, the transmitter and receivers would be on opposite sides of a coal panel or pillar. Using multiple travel paths, the size, type, and location of an anomaly can be determined.

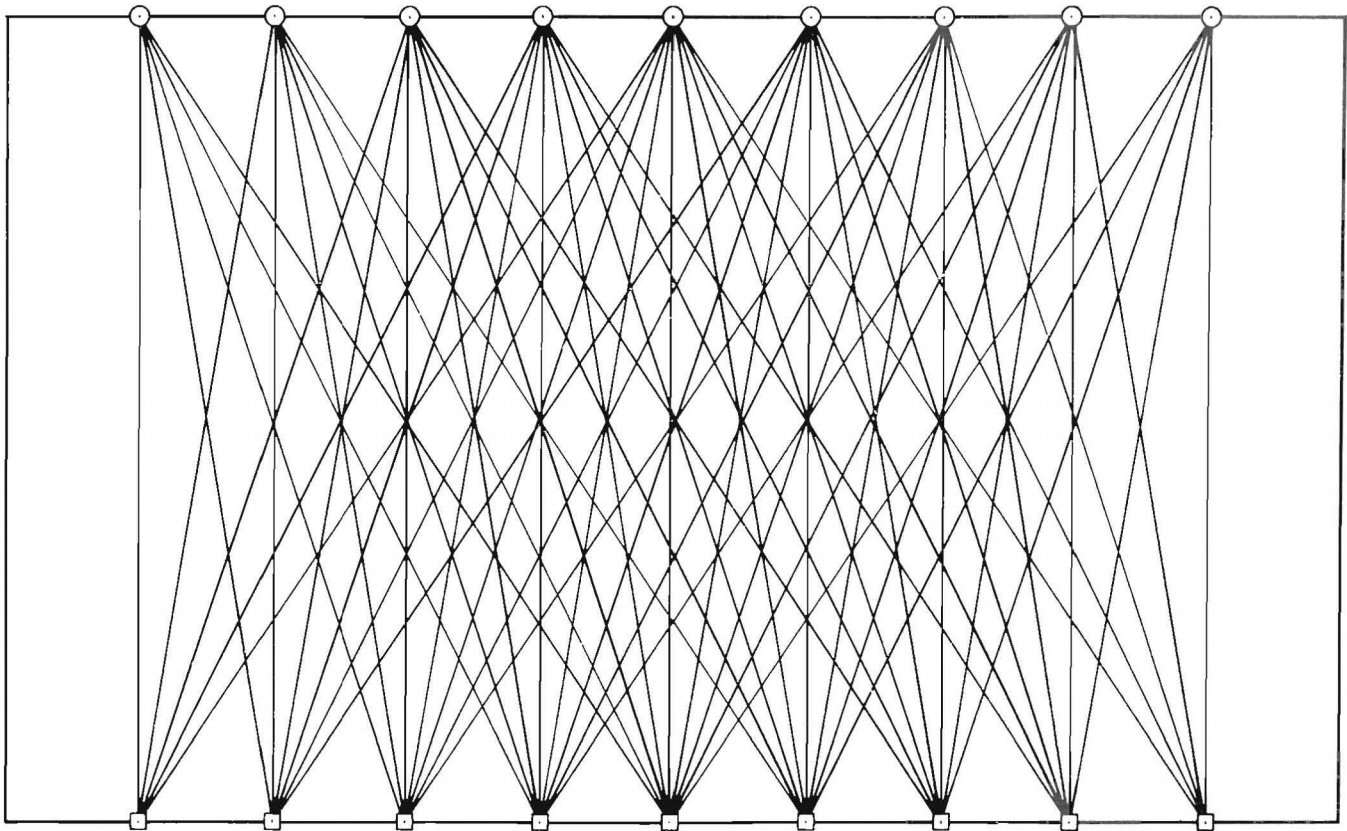
Prior to testing the radar equipment, previous work of this general type was investigated. Several Bureau of Mines research centers have been working on related research in recent years. At the Denver Research Center, investigations have been made involving an overview of several electromagnetic geophysical methods (10-11), and pulse radar has been used to detect sulfides and fractures in an abandoned mine. At the Tuscaloosa Research Center, ground-penetrating radar has been used successfully for a study of mine roof control, and other investigations of near-face hazard detection have also been completed (2, 13). A similar application was tested at the National Bureau of Standards for the Bureau of Mines. In this research, microwave measurements were used to determine coal layer thickness on samples between 10 and 40 cm thick (6). The Pittsburgh Research Center is currently developing a program in geotomographic hazard detection. Anomalies have been detected and imaged by transmitting electromagnetic steady-state carrier waves through coal.

Lawrence Livermore Laboratory (LLL) investigators have been involved in the research and development of electromagnetic cross-borehole probing or transillumination techniques. They have devised methods for looking at two types of anomalies within the host medium (9, 12). The first is a tomographic method for detecting and locating low-contrasting anomalies. "Low contrasting" as used in this context implies electrical properties similar to those of the host rock. The second method is for the detection of high-contrast zones, such as a void within the host rock, using a shadowing technique (5). Also, both seismic and electromagnetic cross-borehole probing have been used successfully to detect regularly shaped cavities with competent surrounding rock (1). Both methods are well documented, and only details, when needed, will be discussed.

The LLL transillumination methodology has been developed specifically for cross-borehole configurations, and direct transfer of that methodology to in-seam

³Underlined numbers in parentheses refer to items in the list of references preceding the appendix at the end of this report.

Transmitter locations



Receiver locations

FIGURE 1.—Model transillumination configuration.

methods is not possible. This is due to a number of differing parameters between the borehole methods and the in-seam radar methods. Some of the major differences that may affect direct transfer of the technology are antennas, geometries, media, and coupling. It is instructive to examine general differences in parameters and to discuss the possible effects these differences may have on the direct transfer of the previous technology.

Antennas:

Borehole.--The LLL borehole probes used dipole antennas.

In-seam.--In-seam radar methods now employ bow tie antennas to increase the capture area.

Concerns.--The major concern is the difference in radiation patterns. For amplitude tomography, it is necessary to

correct the amplitude data for spreading loss from the antenna. For the dipole, a $1/r$ ($r = \text{radius}$) relationship is used, but it has yet to be determined if that relationship can be accurately used for bow tie antennas within a coal seam.

Geometries:

Borehole.--Both antennas are usually vertically polarized and are moved in a plane parallel to the polarization.

In-seam.--Antennas can be placed in any polarization orientation; for maximum penetration, polarization normal to the bedding is preferred. Movement of the antennas will usually be in a plane normal to the polarization.

Concerns.--The correction for radiation patterns will differ from that used in the borehole configuration. Also, the manual placement of antennas on the coal

rib or face for the in-seam method does not assure constant polarization orientation and thus may introduce errors.

Media:

Borehole.--Previous work has assumed homogeneous isotropic media.

In-seam.--Coal is an anisotropic medium usually bounded by layers more conductive than the coal.

Concerns.--In coal, antenna orientation will affect the amplitude measurements.

Coupling Note that the coal-bounding layers may influence amplitude measurements:

Borehole.--The antenna and borehole wall separation is fairly uniform; therefore, coupling between the antenna and the medium is assumed a constant.

In-seam.--The rib or face texture in a coal seam is unlikely to be uniform;

therefore, the distance between the antenna and the medium will vary.

Concern.--Coupling between the antenna and the medium will vary and thus affect the accuracy of the data.

Based on these concerns, three major research objectives were laid out for the development of practical and reliable in-seam transillumination methods; as follows:

1. To evaluate the probable accuracy of amplitude and time data taken in-seam using present instrumentation and measuring procedures.

2. To determine the detectability of hazards as a function of measurement accuracy and relative size using a transillumination method.

3. To develop and test transillumination techniques for detecting and mapping in-seam mining hazards.

ACKNOWLEDGMENTS

The authors wish to thank XADAR Corp. of Springfield, VA, for assistance with

the operation of the synthetic pulse radar system.

EVALUATION OF PROBABLE ACCURACY

For some transillumination methods, detectability is directly related to the accuracy one can achieve by measuring amplitude and/or time data. For any in-seam method to be useful for hazard detection, it must be practical as well as sufficiently accurate. Measurement accuracy may be significantly affected by conditions such as instrumentation accuracy, physical characteristics of the coal seam, and the measurement procedures. It will be assumed that instrumentation and measurement procedures, if inadequate, can or will be evolved to the point where they meet the needed criteria. The physical characteristics of the seam, rib, or face are more difficult, if not impossible, to change, and alteration of these characteristics would normally be impractical.

Tests were conducted first to determine the accuracy of the instrumentation and then to determine the effects the physical parameters of the seam, face, or rib may have on the measurements. For each

test, standard measurement procedures that were considered adequate and practical were used (14). The tests are broken down into two categories: air tests and coal tests. The test results are presented below.

AIR TESTS

The tests were conducted in air to provide data about the instrumentation and its accuracies. The instrumentation, which is described in more detail in the appendix, was a short-pulse radar unit using "off the shelf" laboratory equipment and notched bow tie antennas.

The tests were conducted in an open, flat field, making certain that no return signal from possible reflectors could be detected in the time window used for recording the waveforms. The antennas were placed on easels as shown in figure 2. The easels were 1 m high, causing the center of the 1-m antennas to be 1.5 m above the ground when they were vertically polarized and 1.25 m above the

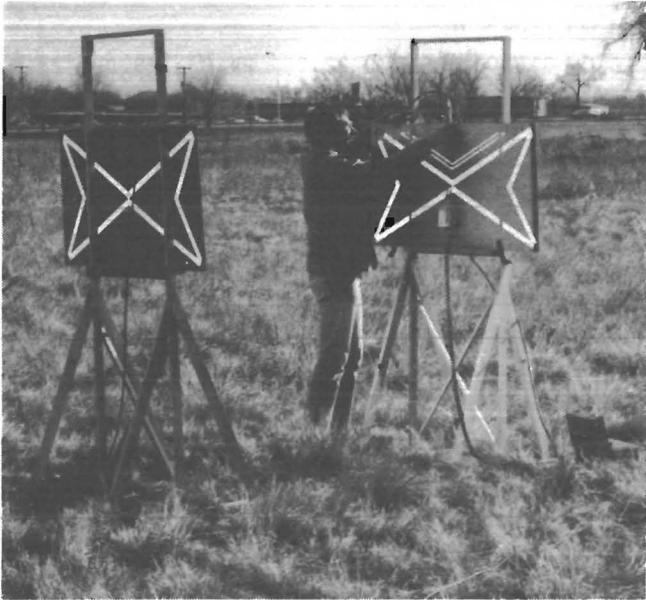


FIGURE 2.—Antennas and easels used for the air tests. Antennas are shown in a horizontal position.

ground when they were in a horizontal polarization configuration.

A test grid (fig. 3) was laid out using measuring tapes and spray paint. The assumed accuracy of the measurements was considered to be within ± 0.1 m. For the air tests described here, the transmitter antenna was placed vertically polarized at the location mark. For each measurement, 16 short-pulse waveforms were digitized, averaged, and recorded on magnetic tape. Each waveform consisted of 1,024 points or elements with a sample interval of 0.195 ns per element.

The four tests to be described are (1) normal moveout, (2) parallel moveout, (3) circular test at a 16-m radius, and (4) receiver rotational test.

Air Test 1: Normal Moveout

This test layout is shown as test 1 in figure 3. The antennas faced each other, and both were vertically polarized. The receiver was moved in 2-m increments from 4 to 26 m. Figure 4 shows a variable wiggle plot of the recorded waveforms.

The first peak or trough after the first break was chosen as a reference from which the time and amplitude data were picked. This peak was chosen due to its ease of detection and due to the fact that it would be the least likely point

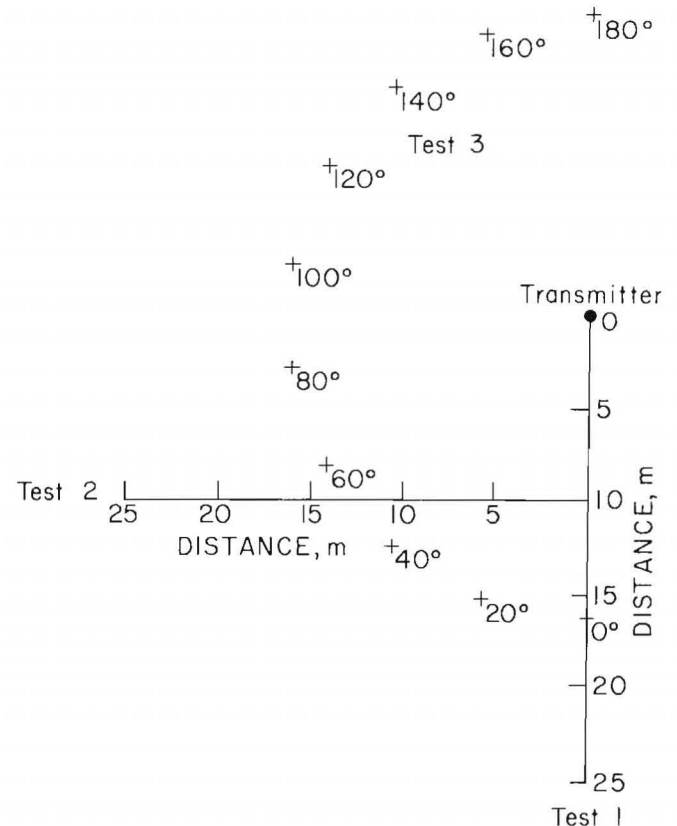


FIGURE 3.—Air test grid. In test 1 the receiver is moved along the vertical axis; in test 2, along the horizontal axis; and in test 3, along the semicircle.

along the waveform to be superimposed with later arriving signals.

Table 1 shows the time and amplitude of the first peak. The time is given in elements or sample number. Actual time can be computed by the relationship

$$\text{time} = \text{element number} \times \text{sample interval.}$$

The time data and best fitted curve of those data are plotted in figure 5. The data curve is linear and is described by the equation

$$y = 110.850 + 16.643 x,$$

where y = time in elements,

and x = distance in m.

The correlation between the fit and data is equal to 1.000. The y intercept can be thought of as a system time delay.

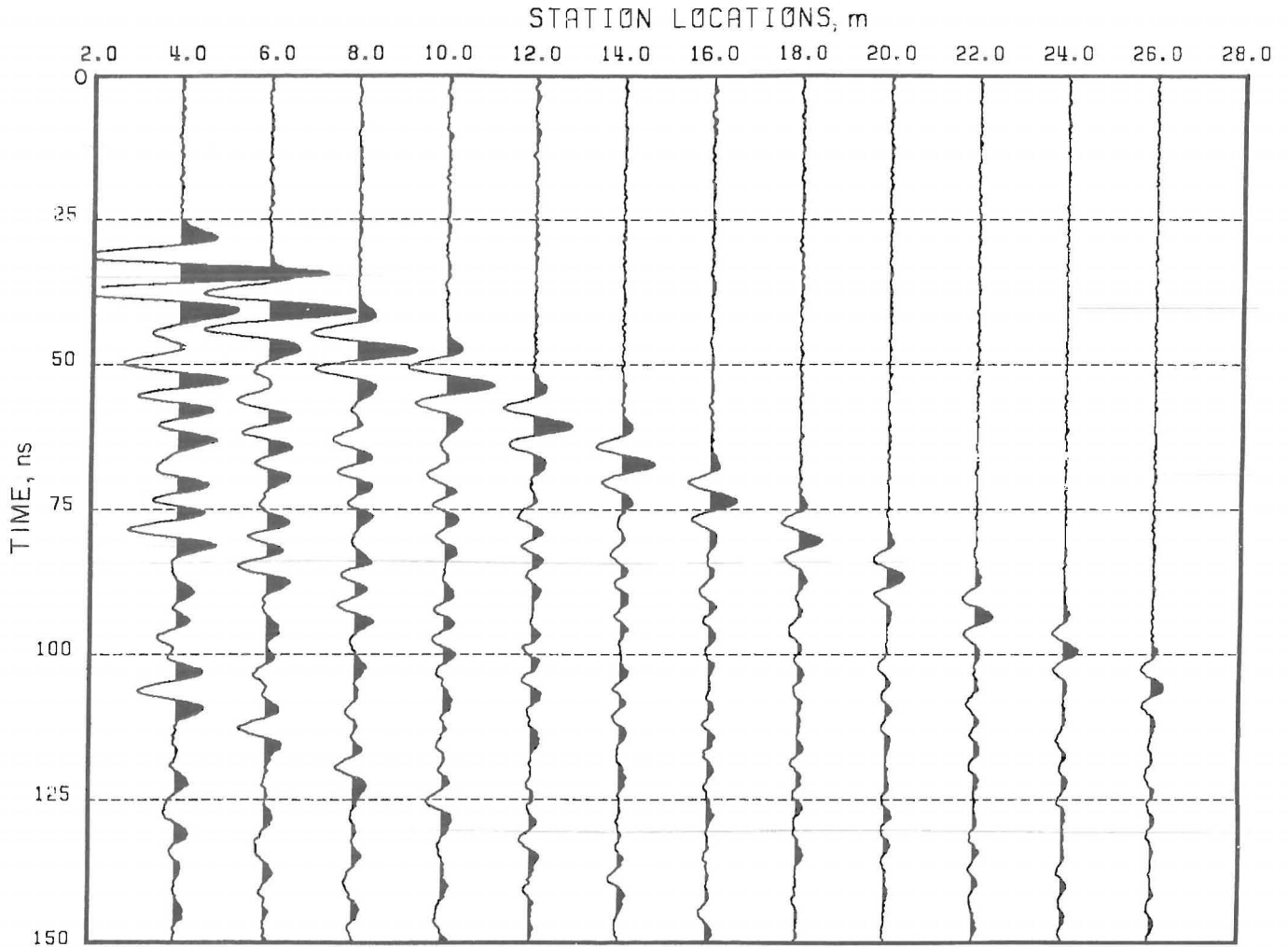


FIGURE 4.—Computer plot of recorded waves from air test 1. The location units in meters indicate the distance from the transmitting antenna to the receiving antenna.

TABLE 1. - Air test 1: Normal moveout in air

Dis- tance, m	Time, element ¹		Amplitude, mV		Dis- tance, m	Time, element ¹		Amplitude, mV	
	Measured	Fitted ²	Measured	Fitted ³		Measured	Fitted ²	Measured	Fitted ³
4.0	177	177	161.8	168.1	16.0	377	377	28.12	28.16
6.0	210	211	94.55	99.70	18.0	412	410	25.14	24.19
8.0	245	244	66.83	68.81	20.0	444	444	18.09	21.12
10.0	275	277	52.20	51.42	22.0	480	477	18.72	18.68
12.0	311	311	41.90	40.80	24.0	509	510	16.36	16.70
14.0	345	344	34.66	33.45	26.0	541	544	13.62	15.06

¹ element = 0.195 ns. ² $y = 110.850 + 16.643 x$. ³ $y = 1.004 x^{-1.289}$.

The inverse slope and time interval yield a velocity of 3.08×10^8 m/s, a 2.7% error on the expected velocity in air of $c = 3.00 \times 10^8$ m/s. The error was computed by

$$\text{error} = (v-c)/c \times 100\%$$

where v = computed velocity in m/s

and c = velocity of light in m/s.

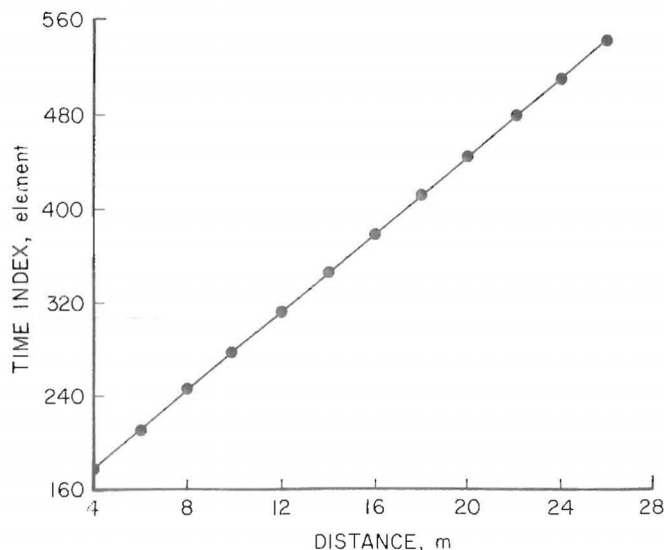


FIGURE 5.—Air test 1, measured time versus distance and best fitted curve. Time in elements = $110.850 + 16.643 \times \text{distance}$ in m. One system time element equals 0.195 ns.

The standard error of estimate, $Sy \cdot x$, of y on x was computed using the general equation for small sample size:

$$\left(\frac{\sum (y - y_{est})^2}{n-2} \right)^{1/2}$$

where y = measured value,

y_{est} = value computed from the curve,

and n = number of samples

For the time data the standard error of estimate is equal to 1.73 elements.

The amplitude data and the best fitted curve describing the data are shown in figure 6. The equation for the fit is

$$y = 1.004 x^{-1.289}$$

where y = amplitude in V

and x = distance in m

The correlation coefficient for the fitted power curve and the data is equal to 0.997, and the standard deviation is 5.88%

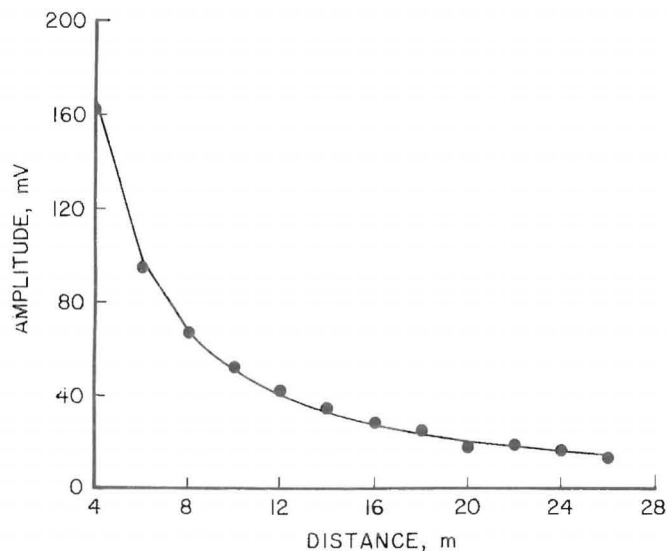


FIGURE 6.—Air test 1, measured amplitude data and best fitted curve. Amplitude in mV = $1,004 \times \text{distance in m}^{*-1.289}$.

Air Test 2: Parallel Moveout

This test layout is shown as test 2 in figure 3. The receiver antenna was moved parallel to the plane of the transmitting bow tie antenna in 1-m steps. This configuration is the one most likely to simulate an actual transillumination survey. The amplitude and time data, and the best fitted data, based on the first peak, are given in table 2. Figure 7 shows the plotted time data and the best fitted curve. The correlation factor for the curve is 1.00, and the equation for the fitted linear curve is

$$y = 84.707 + 17.167 x$$

where y = time in elements

and x = distance in m.

The inverse slope and the sample interval of 0.195 ns per element yield a velocity of 2.98×10^8 m/s, which is within 0.67% error of the assumed velocity of 3.00×10^8 m/s. Further analysis of the data yields a standard deviation of 0.256% and a standard error of estimate of y on x equal to 1.45 elements.

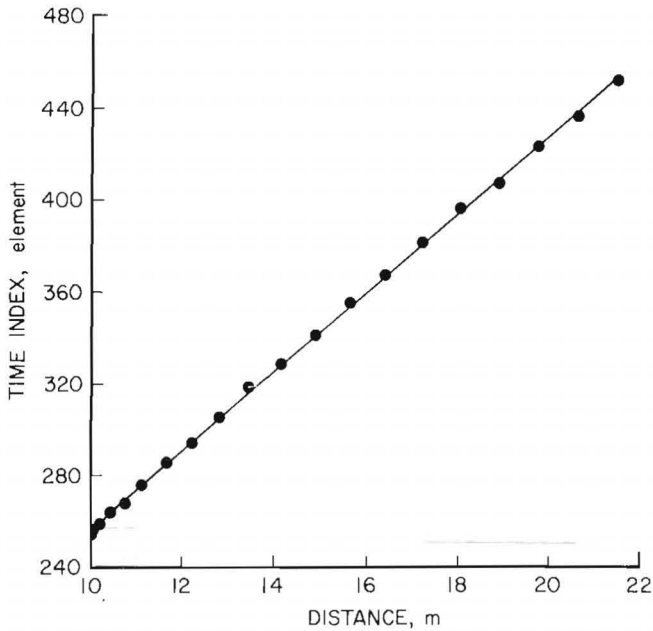


FIGURE 7.—Air test 2, measured time versus distance and best fitted curve. Time in elements = $84.707 + 17.167 \times \text{distance}$ in m. One system time element equals 0.195 ns.

Test 2 amplitude data are plotted with the best fitted power curve in figure 8. The equation for the fit was determined to be

$$y = 0.994 x^{-1.378}$$

where y = amplitude in V

and x = distance in m.

Correlation of the data to fit was computed as 0.978 with a standard deviation equal to 3.643%

Air Test 3: Circular Test

This test is shown as test 3 in figure 3. In this test we moved the receiver in a circle around the transmitting antenna. The face of the receiving antenna was kept tangential to the circle, and the transmitting antenna was kept stationary. The radius of the circle was 16 m. The data for the test are presented in table 3. The average time is 370 elements with a standard deviation of 1.96

TABLE 2. - Air test 2: Parallel moveout test

Station	Distance, m	Time, element ¹		Amplitude, mV	
		Measured	Fitted ²	Measured	Fitted ³
0.0	10.00	254	256	44.80	41.63
1.0	10.05	256	257	45.51	41.34
2.0	10.20	259	260	39.08	40.52
3.0	10.44	264	264	42.23	39.23
4.0	10.77	268	270	37.03	37.58
5.0	11.18	276	275	33.70	35.97
6.0	11.66	286	285	30.29	33.68
7.0	12.21	294	294	29.52	31.63
8.0	12.81	305	304	26.46	29.60
9.0	13.45	318	316	27.64	27.65
10.0	14.14	328	327	24.28	25.82
11.0	14.89	341	340	27.17	24.10
12.0	15.62	355	353	22.76	22.52
13.0	16.40	367	366	23.51	21.05
14.0	17.21	381	380	20.89	19.71
15.0	18.03	396	394	19.00	18.48
16.0	18.87	407	409	17.70	17.36
17.0	19.72	423	423	14.38	16.33
18.0	20.59	436	438	14.92	15.39
19.0	21.47	452	453	15.10	14.52

¹1 element = 0.195 ns.

² $y = 84.707 + 17.167 x$.

³ $y = 0.994 x^{-1.378}$.

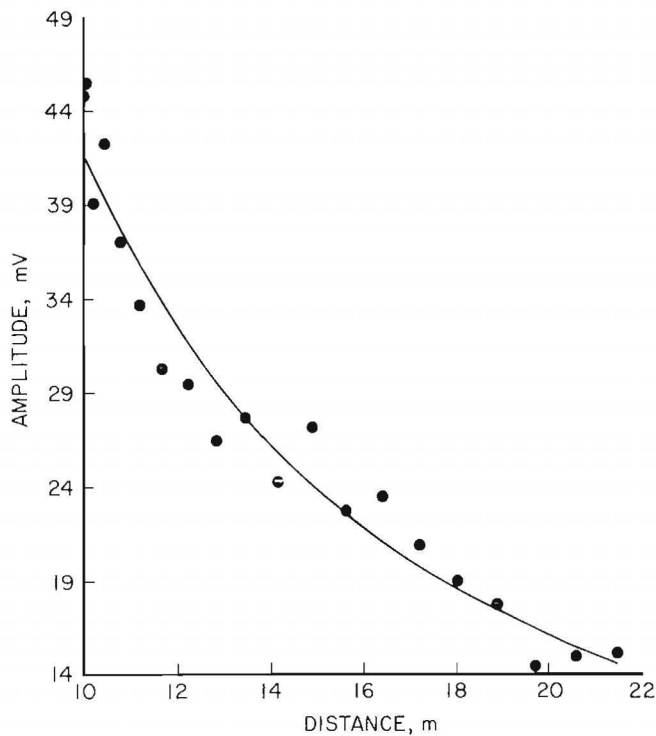


FIGURE 8.—Air test 2, measured amplitude data and best fitted curve. Amplitude in mV = $994 \times \text{distance in m}^{*-1.378}$.

elements. No correction for time delays has been applied to the data, resulting in a difference between measured time versus actual expected time for a travel path of 16 m in air. The average amplitude value is 2.623×10^{-2} V with a standard deviation of 0.2171×10^{-2} V.

Air Test 4: Receiver Rotation

During this test the receiver was placed at the 16-m mark parallel to the transmitter. We then rotated the receiver from a vertical to a horizontal polarization in 10° increments. The angle was measured using a protractor and a pendulum mounted on the antenna. Table 4 shows the amplitude variations.

The results of the air tests were as expected, except for the 2.7% velocity error in the first test. We speculate that this error may be due to drifting of the trigger level within the instrumentation. In practice, an instrument accuracy of 1% should be achievable.

TABLE 3. - Air test 3: Circular air test

Station, deg	Time, element ¹	Amplitude, mV
0.0	366	28.27
10.0	370	26.69
20.0	370	26.43
30.0	369	27.24
40.0	371	25.23
50.0	371	24.77
60.0	372	24.79
70.0	372	23.07
80.0	371	24.32
90.0	373	22.22
100.0	373	24.78
110.0	370	24.13
120.0	369	26.10
130.0	367	27.62
140.0	371	26.52
150.0	370	29.13
160.0	370	30.63
170.0	372	28.29
180.0	367	28.21

¹1 element = 0.195 ns.

TABLE 4. - Air test 4: Antenna rotational test

Station, deg	Time, element ¹	Amplitude, mV
0.0	285	59.93
10.0	285	57.57
20.0	285	57.62
30.0	285	58.33
40.0	285	53.34
50.0	285	45.95
60.0	284	37.39
70.0	285	25.52
80.0	286	12.71
90.0	284	4.15

¹1 element = 0.195 ns.

For air tests 1 and 2, a $1/r$ relationship would be expected if the antennas were in homogeneous air. However, ground and field effects may alter the expected values. Air test 3 helps to demonstrate the unsymmetrical radiation patterns from a bow tie antenna. This finding must be considered for transillumination techniques requiring spreading corrections.

COAL TESTS

The same short-pulse instrumentation tested in air was then taken to a coal mine in an attempt to discern the effects the physical constants of the mine and coal seam would have on determining accurate amplitude and velocity measurements. Utah Power and Light cooperated with these tests by providing a test coal pillar at the Deseret Mine near Price, UT.

The experiments were conducted using a square coal pillar approximately 25 m on a side. Due to the high attenuation factor of the coal, penetration across the pillar was not possible without adding a previously untested amplifier to the instrumentation. Consequently, two adjacent sides of the pillar were used for the experiments. A plan view of the test configuration is shown in figure 9. As in the air tests, the distance measurements were made using a measuring tape, and locations were marked using spray paint.

The three experiments used to evaluate the determination of expected accuracy in measurements are (1) receiver antenna rotation, (2) parallel moveout from 5 to 25 m, and (3) parallel moveout from 25 to 5 m.

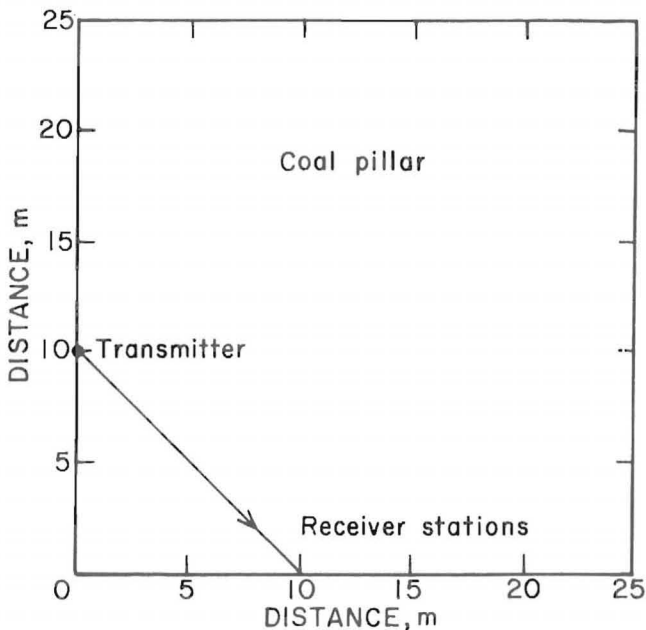


FIGURE 9.—Plan view of coal mine test pillar.

For all three tests, the transmitter was vertically polarized at the 10-m location as marked in figure 9, and the sample interval was 0.488 ns per element. An average of 16 waveforms were recorded for each measurement.

Coal Test 1: Rotation
of Receiver Antenna

The purpose of this test is to evaluate the effects that antenna rotation would have on the measurements. Coal is anisotropic, and waves from vertically polarized antennas are less attenuative than those from horizontally polarized antennas (8). Changes in polarization, either by accident or by design, could adversely affect the measurements.

This test was conducted at the receiver 10-m mark. The receiver antenna was rotated in 5° increments from 0° to 90°. The recorded waveforms are shown in figure 10. The amplitude and time data are presented in table 5. Figure 11 is a plot of the amplitude data. The large dropoff in amplitude between 0° and 5° is probably due more to the change in

TABLE 5. - Coal test 1: Antenna rotational test

Station, deg	Time, element ¹	Amplitude, mV
0.0	211	200.9
5.0	211	126.3
10.0	212	151.8
15.0	213	151.3
20.0	213	168.8
25.0	213	167.9
30.0	213	169.6
35.0	214	176.5
40.0	214	166.6
45.0	214	150.9
50.0	213	164.8
55.0	214	155.2
60.0	214	157.0
65.0	213	141.9
70.0	214	124.9
75.0	214	121.3
80.0	213	89.68
85.0	213	68.70
90.0	213	46.13

¹1 element = 0.4883 ns.

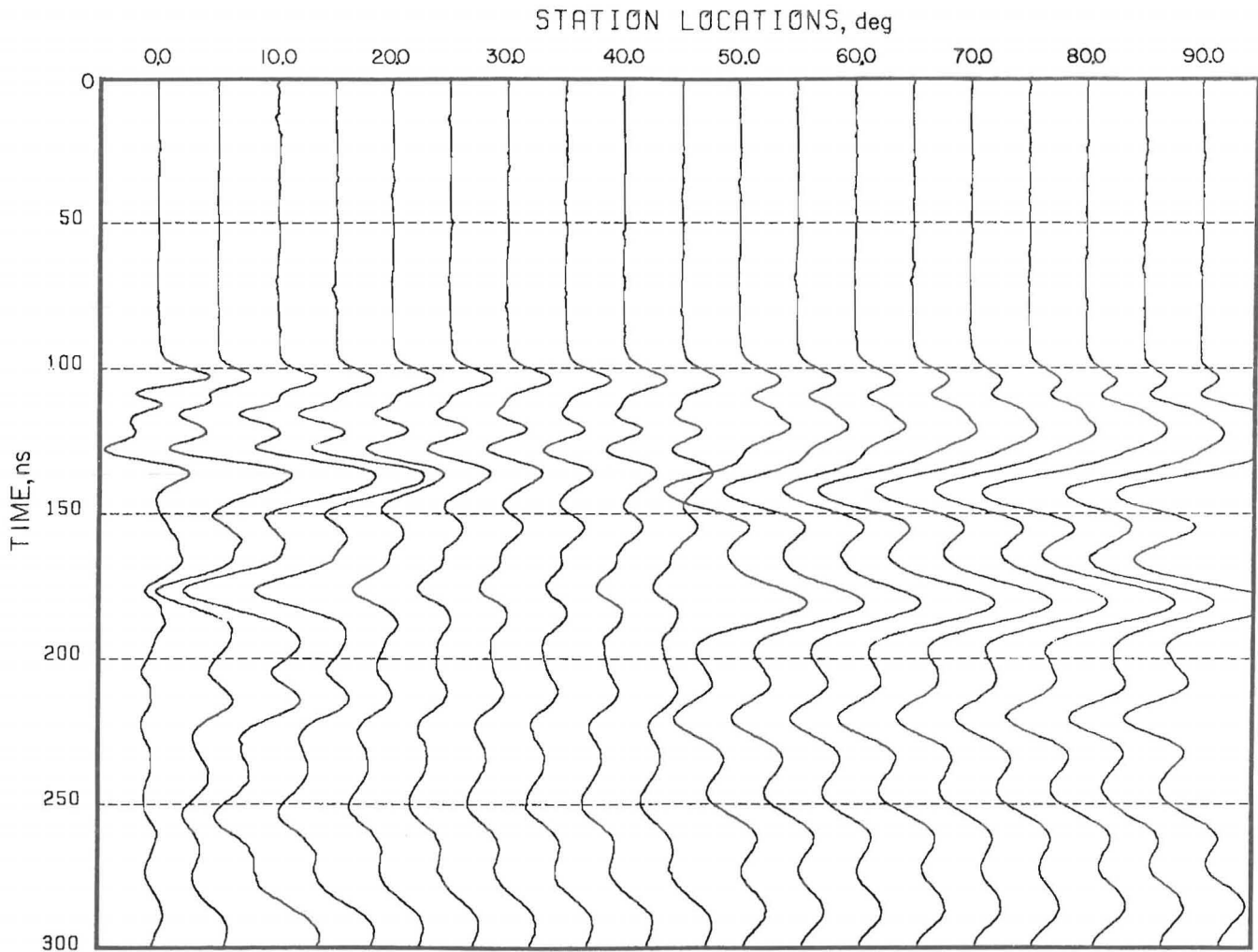


FIGURE 10.—Coal test 1, rotation of receiver antenna. Computer plot of the recorded waves ranging from 0° rotation on the left to 90° rotation on the right.

coupling than to effects due to rotation. That is, in order to rotate the antenna, it was slightly displaced from the rib. For comparison to air test 4, the mean amplitude value is 142.12 mV with a standard deviation equal to 38.63 mV. The amplitude drop from maximum to minimum is 29 dB.

Coal Tests 2 and 3: Moveout Parallel to Coal Rib

The discussion of these two tests is combined because theoretically results should be identical if there is to be repeatability in the measurements. For test 2, we moved the receiver antenna from the 5-m station to the 22-m station in 1-m intervals. The recorded waveforms

are shown in figure 12. In that figure it can be seen that the waveforms become more dispersed with an increase in distance. In fact, the reference peak for the last two waveforms could not be determined, and the data are left blank for stations 19 and 20 in table 6.

In test 3, the process was reversed by moving the receiver antenna from the 20-m station to the 5-m station. The resulting recorded waveforms were similar to those in test 2 and are not shown. The reference peak and best fitted data are presented in table 7.

Figure 13 is a plot of the time data for both test 2 and test 3. The best fitted curve for each set of data is also plotted. For both sets of data the correlation coefficient for the fitted curve

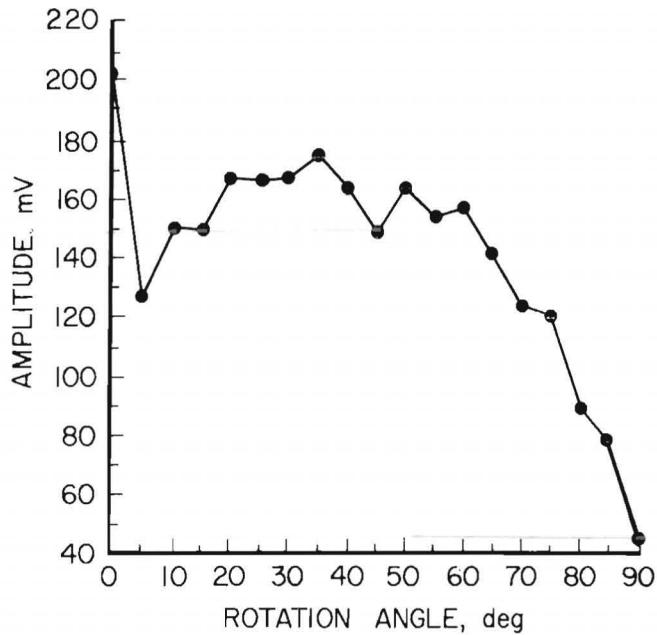


FIGURE 11.—Coal test 1, rotation of receiver antenna. Plot of amplitude versus receiver rotational angle. Amplitude drops off sharply starting at about 60° rotation.

was 0.999. The equations for each curve are

$$\text{Test 2: } y = 33.713 + 12.328 x$$

$$\text{Test 3: } y = 36.646 + 12.259 x$$

where y = time in elements

and x = distance in m.

The slopes of the two curves are almost identical, and the intercept term can be explained as a change in trigger level in the instrument causing a change in the time delay. The computed velocity for the coal, using the slope and the sample interval of 0.4883 ns, for test 2 is 1.661×10^8 m/s and for test 3 is 1.671×10^8 m/s. For test 2 the mean absolute error is 0.434% with a standard deviation of 0.412%. Test 3 results are 0.426% and 0.304% respectively. The standard error of estimate of y on x for both tests is equal to 1.354 elements.

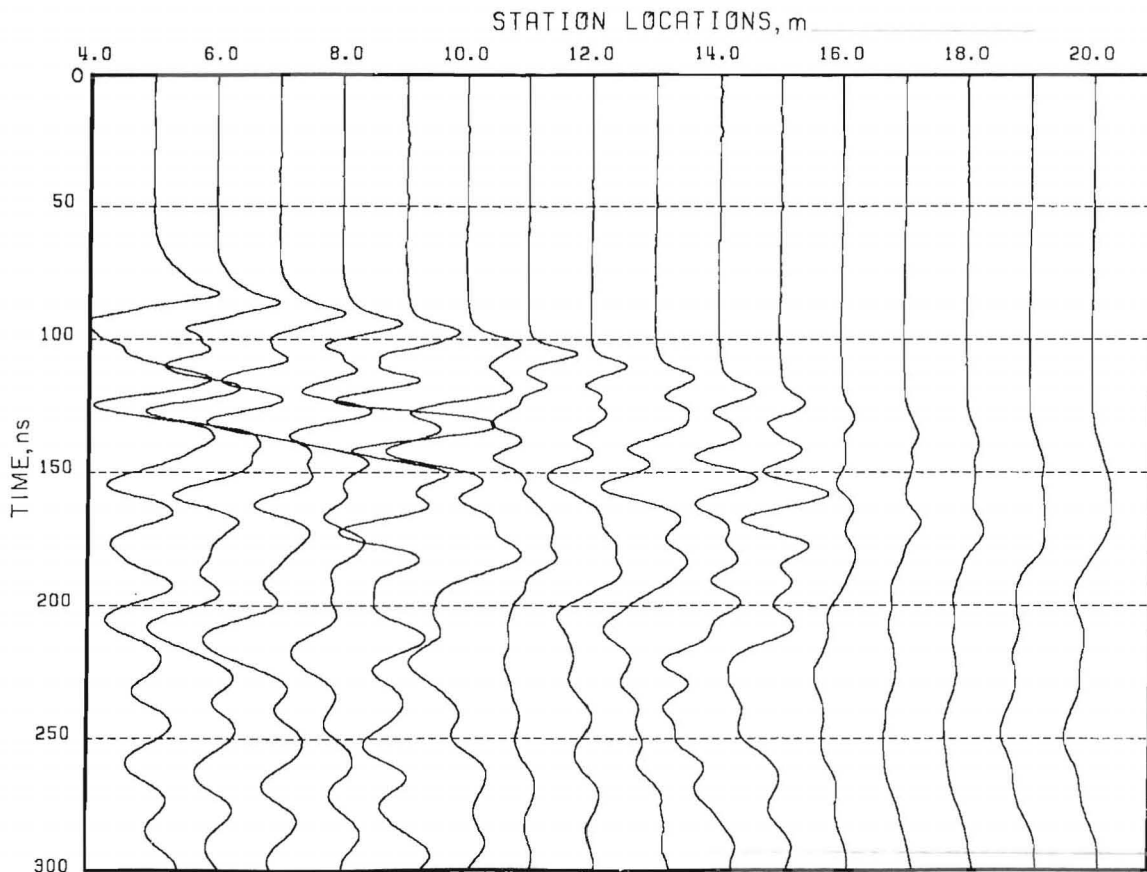


FIGURE 12.—Coal test 2, moveout parallel to coal rib. Computer plot of the recorded waveforms. Distances in meters indicate the position of the receiver antenna along the coal pillar.

TABLE 6. - Coal test 2: Moveout test 1

Station	Distance, m	Time, element ¹		Amplitude, mV	
		Measured	Fitted ²	Measured	Fitted ³
5.0	11.18	170	172	361.9	400.0
6.0	11.66	177	177	355.0	377.7
7.0	12.21	186	184	369.9	353.0
8.0	12.81	193	192	334.3	328.0
9.0	13.45	200	200	303.7	301.8
10.0	14.14	209	208	306.3	275.3
11.0	14.87	216	217	276.9	248.8
12.0	15.62	226	226	197.9	225.5
13.0	16.40	234	236	220.3	196.6
14.0	17.20	246	246	108.6	171.2
15.0	18.03	254	256	142.5	146.4
16.0	18.87	267	266	74.20	122.2
17.0	19.72	278	277	82.46	98.7
18.0	20.59	288	288	73.70	75.8
19.0	21.47	NA	NA	NA	NA
20.0	22.36	NA	NA	NA	NA

NA Not available.

¹1 element = 0.4883 ns.

² $y = 33.713 + 12.328 x$.

³ $y = 1.682 + -0.531 \ln(x)$.

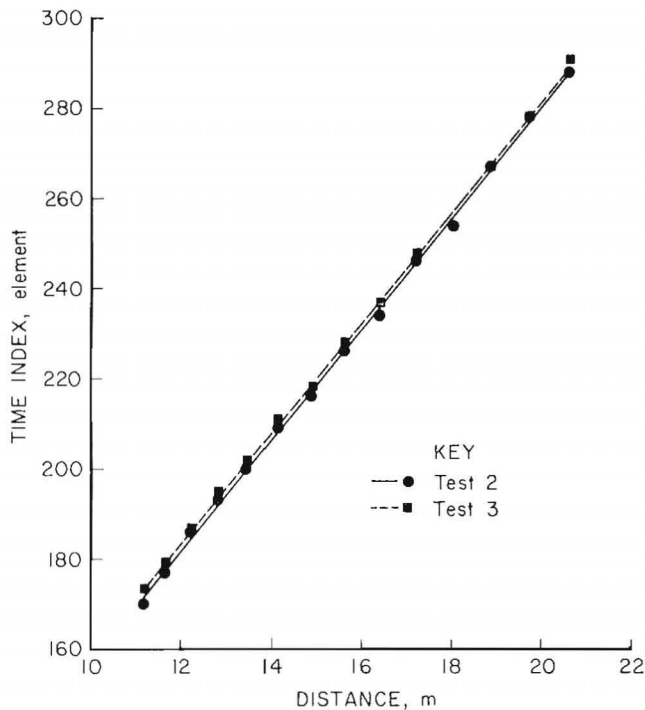


FIGURE 13.—Coal test 2 and 3, measured time versus distance and best fitted curves. For test 2, time in elements = $33.713 + 12.328 \times$ distance in m; for test 3, time in elements = $36.646 + 12.259 \times$ distance in m. One system time element equals 0.488 ns.

The amplitude data and the logarithmic fitting curves for tests 2 and 3 are plotted in figure 14. The equations and correlation coefficients, ρ , for each test are--

$$\text{Test 2: } y = 1.682 - 0.531 \ln(x)$$

$$\rho = 0.970$$

$$\text{Test 3: } y = 1.822 - 0.595 \ln(x)$$

$$\rho = 0.986$$

where y = amplitude in V

and x = distance in m.

The mean absolute error for test 2 is 10.806% with a standard deviation of 10.168%; test 3 results are 7.733% and 4.250% respectively.

Coal tests 2 and 3 clearly showed that repeatability is hard to achieve. In fact, the mean difference in amplitudes is -19.11% with a standard deviation of 23.35%. This lack of repeatability could be partly due to differences in coupling.

TABLE 7. - Coal test 3: Moveout test 2

Station	Distance, m	Time, elements ¹		Amplitude, mV	
		Measured	Fitted ²	Measured	Fitted ³
5.0	11.18	173	173	416.4	385.6
6.0	11.66	179	180	357.3	360.5
7.0	12.21	187	186	330.7	333.3
8.0	12.81	195	194	276.2	304.8
9.0	13.45	202	202	302.8	275.4
10.0	14.14	211	210	201.2	216.0
11.0	14.87	218	219	210.1	216.0
12.0	15.62	228	228	204.4	186.6
13.0	16.40	237	238	145.8	157.6
14.0	17.20	248	247	143.0	129.1
15.0	18.03	255	258	96.48	101.3
16.0	18.87	267	268	80.50	74.21
17.0	19.72	279	278	52.54	47.84
18.0	20.59	291	289	21.41	22.20
19.0	21.47	NA	NA	NA	NA
20.0	22.36	NA	NA	NA	NA

NA Not available.

¹1 elements = 0.4883 ns.

²y = 36.646 + 12.259 x.

³y = 1.882 + -0.595 ln(x).

Rotation of the antennas also can contribute to the error; this error can be caused both by the use of polarized antennas (air test 4) and by the medium's anisotropic characteristics (coal test 1). Slight rotation of the antennas should be tolerable. The curves for coal tests 2 and 3 would also be expected to be exponential and not logarithmic, even allowing for the $1/r$ spreading factor.

EVALUATION CONCLUSIONS

Analysis of the data leads to two conclusions. One is that time data can be taken with good accuracy and are generally immune to external factors. The second is that before using amplitude measurements, as LLL does (9), more work will have to be done to determine how the amplitude-attenuation relationship will (1) be affected by the coal medium and (2) be best used to complement the time-velocity data for maximum information gain.

For all of the tests but one, the time data behaved as was theoretically expected for the instrumentation used. The errors encountered were usually no worse

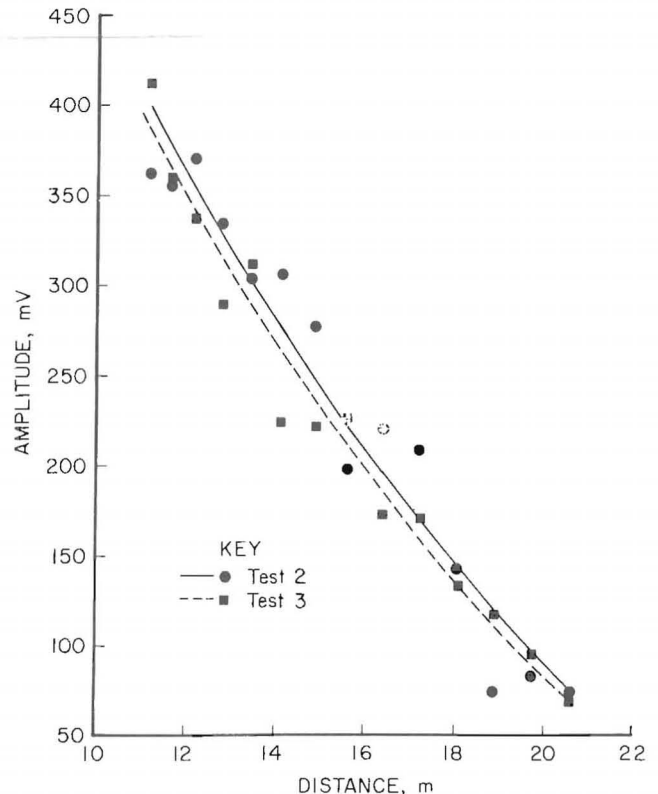


FIGURE 14.—Coal tests 2 and 3, measured amplitude versus distance and best fitted curves. For test 2, amplitude in mV = $1,682 - 531 \ln(\text{distance in m})$; for test 3, amplitude in mV = $1,822 - 595 \ln(\text{distance in m})$.

than the inaccuracies of the distance measurements. The standard error of measurement for the time tests indicates an accuracy of approximately ± 3 elements. Therefore, to achieve the 1% accuracy, the fastest sampling rate possible should be used.

Evaluation of the amplitude data is not as simple as that of the time data. The best-fitted curves contain appreciable error and are not the ones that are theoretically expected. The cause of this error can only be speculated on until further analysis is done.

DETECTABILITY

For low-contrasting anomalies, detectability can be thought of as a function of size and physical properties of the anomaly versus the size and properties of the host medium. That is, for an anomaly to be detected, it must be of sufficient size and/or contrast to alter the measurements being taken. Furthermore, these alterations in measurements should be greater than the possible error so that alteration due to an anomaly can be distinguished from an error in the measurement.

A model was devised to investigate detectability of a low-contrasting anomaly in a host medium. A plan view of that model is shown in figure 15. The host has a thickness of X_1 , a velocity of v_1 , and an attenuation factor of α_1 . The anomaly thickness is X_2 , the velocity is v_2 , and the attenuation is α_2 . A ratio process was then used to investigate changes in time and amplitude due to changes in thickness, velocity, and attenuation. The time ratio t_2/t_1 is computed by the equation

$$\frac{t_2}{t_1} = 1 + \frac{X_2}{X_1} \left[\frac{v_2}{v_1} - 1 \right].$$

The equation for the amplitude ratio A_2/A_1 is

$$\left(-\frac{X_2}{X_1} \left[\frac{\alpha_2}{\alpha_1} - 1 \right] \right)$$

$$A_2/A_1 = e.$$

Other information in the data may also be of possible interest. The first observation is the increase in amplitude of the readings in coal over the readings in air. The cause could be an increase in antenna efficiency and/or a focusing effect due to the coal and roof and floor layers. Another observation is that there is some correlation between the wavelengths of the apparent "ringing" observed in the time-amplitude plots and multiples of either the room size or the seam height, possibly showing resonant and/or wave guide effects.

A set of curves describing the time and amplitude ratios as a function of the thickness ratio were plotted for various velocity and attenuation ratios. Figure 16 is the plot of the time ratios for various velocity ratios with the thickness ratio ranging from 0 to 0.1. Figure 17 shows the amplitude ratios for the same thickness range for various attenuation ratios.

From these plots it is possible to determine the type and size of anomalies that can be detected given the desired error tolerance in the time or amplitude measurements. For example, assuming a

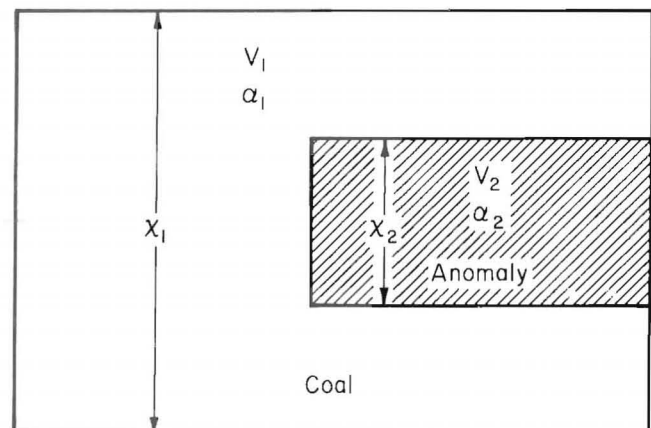


FIGURE 15.—Plan view of coal pillar design used for detectability modeling. Variable x is the width, v is the velocity, and α is the attenuation constant.

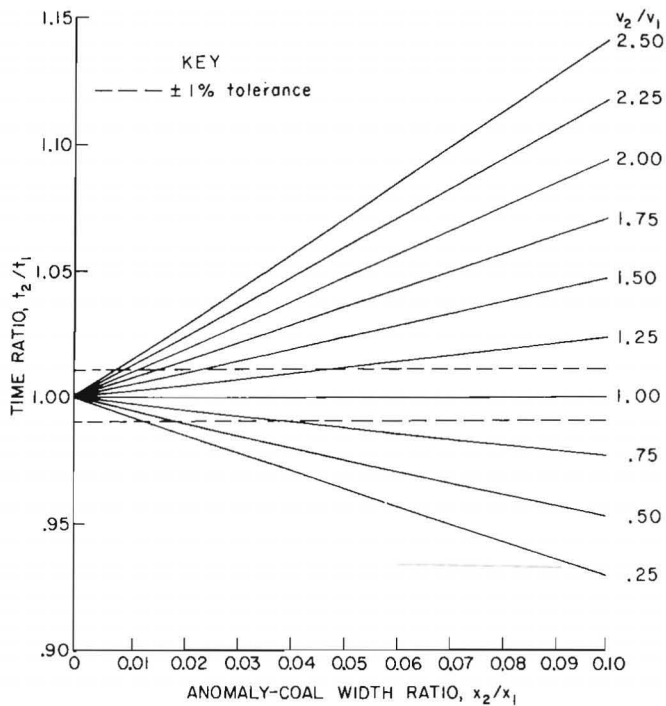


FIGURE 16.—Plot of model time ratio versus width ratio for different velocity ratios.

tolerance of 1% for the time measurements and starting at the point where no anomaly would exist (i.e., time ratio = 1.0), horizontal lines can be drawn at the time ratios 0.99 and 1.01 as shown in figure 16 to represent this error tolerance. All of the velocity ratio points falling between these tolerance lines would not be detectable since they represent time differences that are less than the possible error. For example, to detect a low-velocity anomaly that is 0.038 times the width of the coal column, the

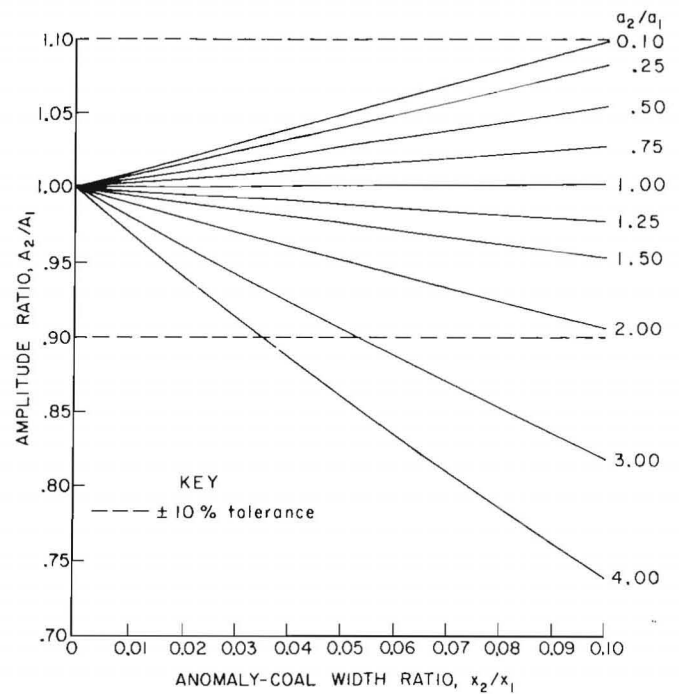


FIGURE 17.—Plot of model amplitude ratio versus width ratio for different attenuation ratios.

velocity ratio of anomaly to coal column would have to be at least 0.75 for the anomaly to be detectable. The same can be done with the amplitude ratios. A 10% tolerance line has been drawn in figure 17 for comparison. In this case, no anomalies with attenuation ratios falling between the line at 0.90 and 1.10 would be detectable, since the amplitude differences are within possible error for the system. Expected attenuation and velocity ratios can be determined or found in published literature (4).

VELOCITY RADAR TOMOGRAPHY

The selection criteria for choosing an appropriate transillumination technique are based on the determination of the type and size of anomalies to be detected. For in-seam surveys, transillumination methods are expected to be conducted on pillars or panels, and the majority of the expected anomalies can be considered as low contrasting to host media and of variable size. Based on this assumption, we felt that a tomography process would provide the best detection capability. But with the present

instrumentation and measuring procedures, it was felt that an amplitude tomography technique would be inaccurate, in terms of both the measurements and the application of the appropriate spreading corrections. However, our studies indicated that time data could be used for development of a tomography process using velocities. We then set out to develop the procedures and techniques required for imaging using velocity tomography.

The work was broken up into three phases: (1) acquiring measurements on a

pillar with a known anomaly, (2) developing required procedures for processing and displaying both short-pulse radar and synthetic-pulse radar data, and (3) modeling the expected results for comparison to the actual data.

PHASE 1: DATA ACQUISITION

The pillar chosen is located at the Bureau's Coal Research Mine in Bruceton, PA. The approximately 8.5- by 17.5-m pillar has a clay vein running through it. A plan view of the pillar and the position of the approximate center of the vein at midseam are shown in figure 18. The vein varies in thickness, but we assumed an average of about 0.5 m for the actual thickness. Also, the vein is not vertical, but dips 50° to 60° . The pillar is small, allowing for comparative tests to be conducted with the short-pulse system used in the earlier tests and the synthetic-pulse radar system.

Synthetic-pulse radar differs significantly from short-pulse radar in that a single frequency is transmitted at a time. The transmitted frequencies of the synthetic-pulse system are in the range of 20 to 160 MHz. The amplitude and phase of each received signal are measured and recorded before the system steps up to the next frequency. The time pulse is then reconstructed by taking the inverse Fourier Transform of the received data.

The measurement procedures were almost identical for both the short-pulse and

the synthetic-pulse systems. The transmitter was positioned and moved along one side of the pillar, and the receiver was positioned and moved along the opposite side. Figure 18 shows a typical set of receiver stations for a given transmitter station. This "two-sided" procedure was chosen over a "four-sided" approach (where measurements are taken using all four sides) because it was felt that this best simulated a procedure that would be required for use on longwall panels.

For the short-pulse test, the transmitter was moved from 2 m to 16 m in 1-m increments. At each transmitter location, the receiver was moved from -5 m to +5 m in 0.5-m increments from the center of the transmitter station location. At the edges, the readings were tapered with the minimum receiver station being set at 1 m and the maximum at 16 m. Figure 19 is a composite of the waveforms in the order in which they were recorded. The first and last waveforms are the trigger signals used to provide time delay corrections to the data. The sample interval for the short-pulse data was 0.1953 ns per element. The synthetic-pulse measurement technique was the same, except that the transmitter was moved from 3 m to 14 m. Figure 20 contains the synthesized waveforms in the order in which they were recorded. The 300-ns arrival times include a 255-ns cable time delay and are therefore not indicative of deep penetration.

PHASE 2: VELOCITY TOMOGRAPHY

Implementation

For the initial development of a tomography method, a back projection technique was decided upon. This technique was chosen because of its ease in implementation, its nonbiasing behavior, and its insensitivity to noise, and because of the favorable results that LLL (9) has using this particular technique on amplitude data.

The back projection is a weighted average technique, making limited assumptions about the coal panel or pillar. For the velocity tomography, the velocity of each

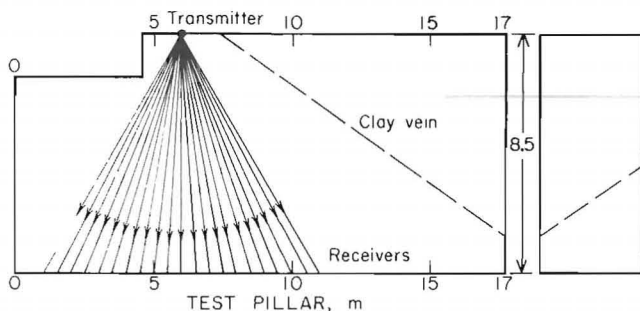


FIGURE 18.—Plan view of Bruceton Coal Research Mine test pillar containing a clay vein. A typical transmitter station and receiver stations are shown.

STATION LOCATIONS

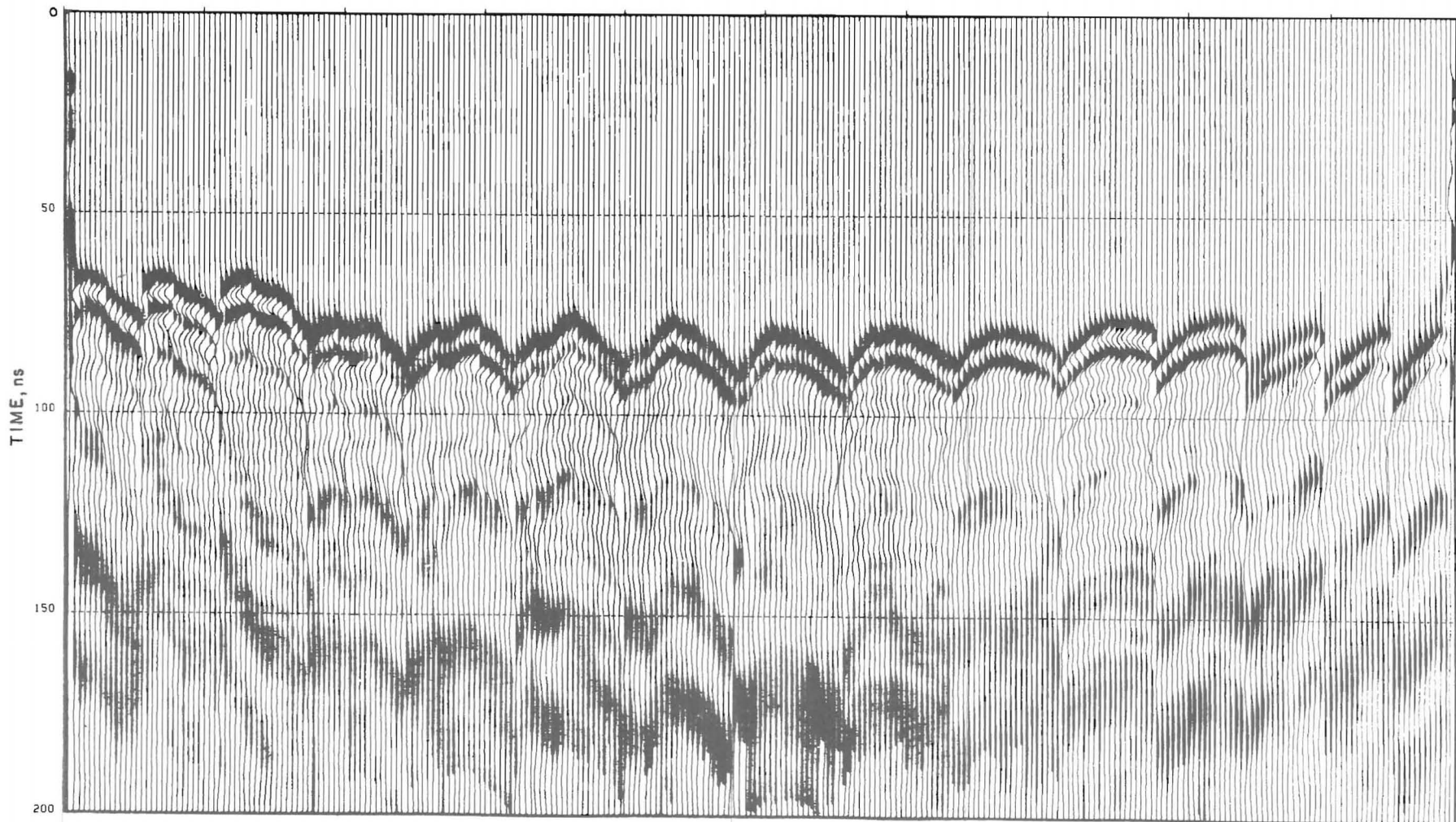


FIGURE 19.—Computer plot of short-pulse waveforms in order they were taken for the tomography scan. Each identifiable "arc" of waveforms represents the time differences involved in going from one transmitter location to different receiver locations across the pillar. The first and last waveforms are trigger signals used for time-delay corrections.

STATION LOCATIONS

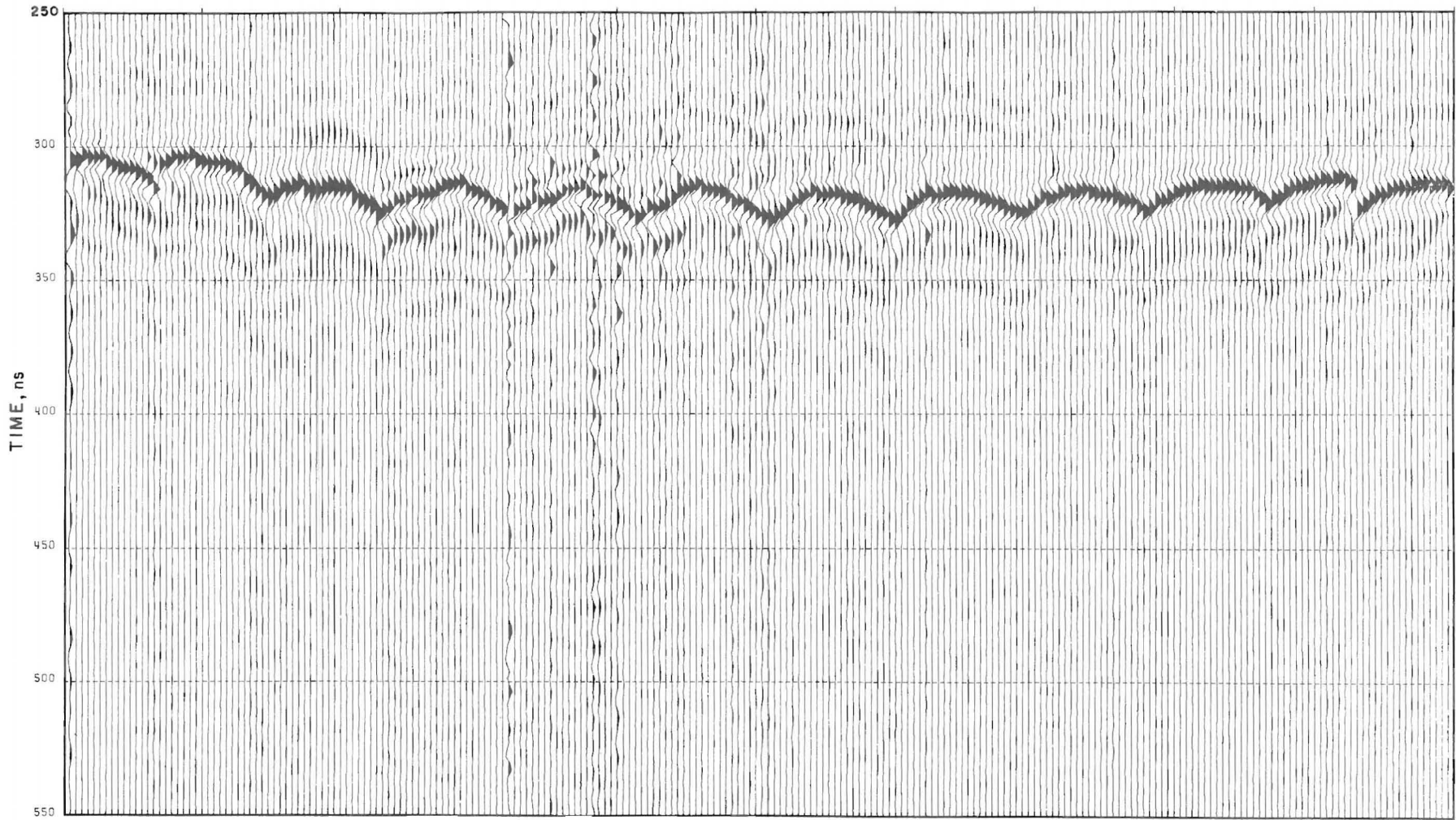


FIGURE 20.—Computer plot of synthetic-pulse waves in order they were recorded. Again, each identifiable “arc” of waveforms represents the time differences involved in going from one transmitter location to different receiver locations across the pillar. A 255-ns cable time delay is present in the data.

travel path passing through the region under investigation is determined. The velocity, V_i , for the i^{th} path is determined from the measured time and distance as

$$V_i = L_i/T_i$$

for path i passing through the media, $i=1,2,\dots,M$ paths

where L_i = measured straight-line travel distance

and T_i = measured time to travel length L_i .

The main assumption made here is that the travel paths are straight lines. This infers that (1) refraction has a minor effect on the travel distances and (2) all the material under investigation has similar electrical properties for the electromagnetic frequencies being used. This, of course, may or may not be the case for a particular investigation.

To implement the back projection technique, a representational region of the coal pillar or panel under investigation is set up and is subdivided into zones or cells. A weighted velocity average is then determined for each cell using the computed velocity for each path passing through the zone. For the k th zone the weighted velocity is

$$\frac{\sum_i V_i L_{ik}}{\sum_i L_{ik}}$$

where V_i is the velocity of transmitter-receiver path i , calculated by dividing the path length by the signal arrival time

and L_{ik} is the distance that transmitter-receiver path i travels through velocity cell k

for all paths i passing through zones k , $k=1,2,\dots,N$ zones. The result is a set of cell velocities, each consisting of an average of velocities of all paths passing through the cell, weighted

according to how much of each path passed through the cell.

Results

For the results to be shown, the representational pillar under test was subdivided into zones 0.5 m square. Figure 21 shows 1-m-square zones and a partial set of travel paths used. The size of the zones is based on the anomaly size, detection capability, statistical significance of the data set within each zone for the averaging process, and convenient output size.

A number of display techniques were tested. The best was a color display of the data wherein color is used to enhance regions of interest. Unfortunately color does not lend itself to publication, so gray scale, line printer, and contour displays are used herein. The standard working display was the line printer output. This display provides a hard copy with fast turnaround which (for this case) can easily be hand contoured. The short-pulse line printer plot is presented in figure 22. Each 0.5-m-square cell is made up of two horizontal characters. The velocity key for each cell is presented and represents velocities between 1.38×10^8 m/s and 1.48×10^8 m/s. Computerized contouring was used on the data, but for a data set of this size and simplicity, hand contouring was found to be adequate. The last display is a gray scale technique wherein the velocity cells are presented as different shades of gray.

Figure 23 is the gray scale tomographic plot of the short-pulse velocity data. In comparison figures 24 and 25 are the line printer and gray scale tomographic plots derived from the synthetic-pulse data.

Before beginning the discussion on interpretation of the results, it is beneficial to compare the short-pulse data to the synthetic-pulse data. When studying any of the plots, there is general agreement between the two data sets. Most of the differences seen are due to the fact that slight velocity gradations are plotted as abrupt changes. There is,

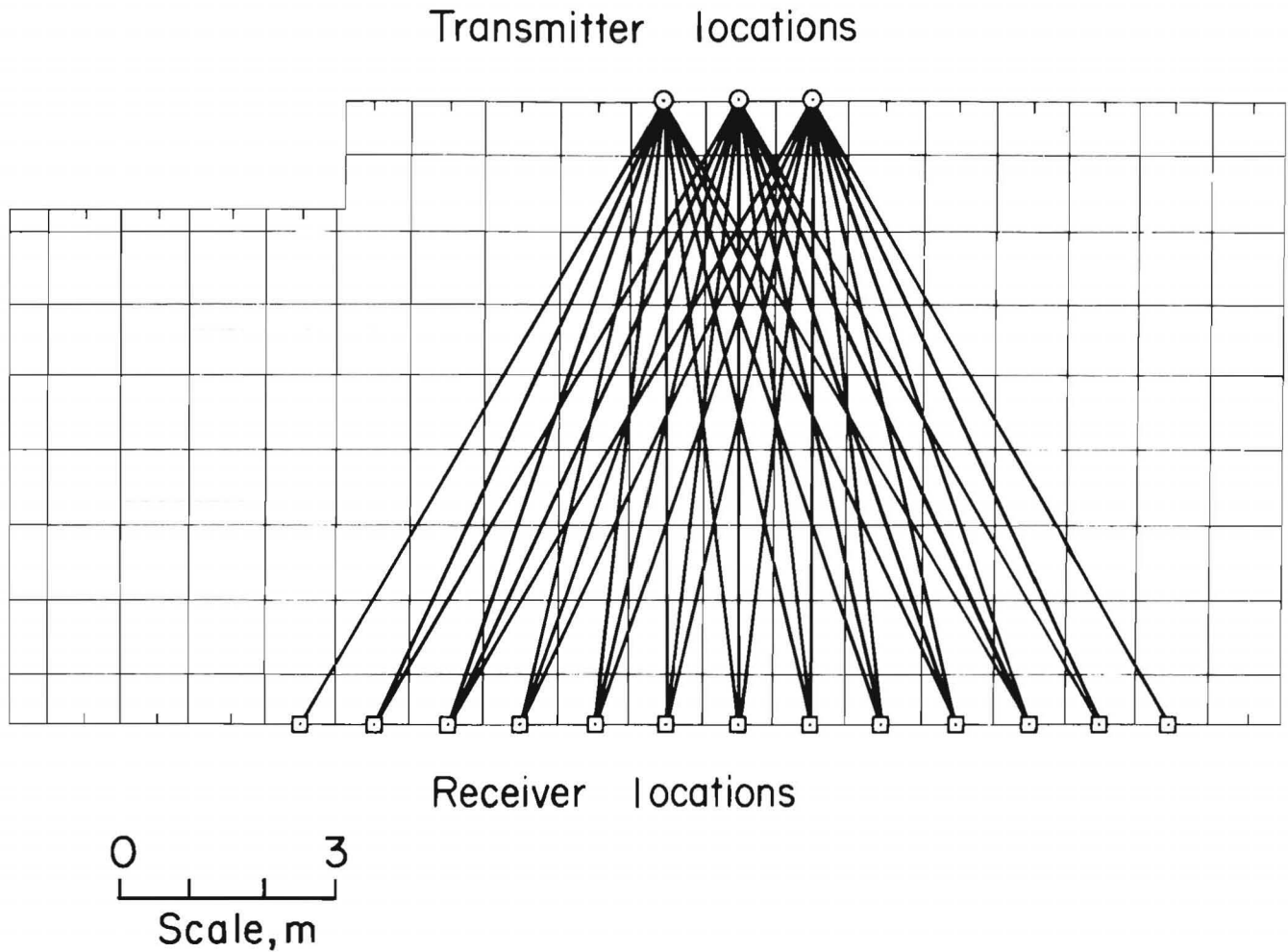


FIGURE 21.—Representative tomographic pillar divided into 1-m-square cells or zones. Three transmitter stations and some of the receiver stations for each are shown. A weighted average of the velocities of the different paths is used to determine the velocity within the cell.

however, one major contradiction between the two data sets. This is that the upper right-hand corners have opposite velocity trends. The short-pulse data set indicates a low-velocity region in that area, whereas the synthetic-pulse data set indicates a high-velocity region.

This contradiction is most likely due to recording errors that occurred in the synthetic system during the last two transmitter stations, as well as to the fact that fewer transmitter stations were used in the velocity calculation for the synthetic-pulse system.

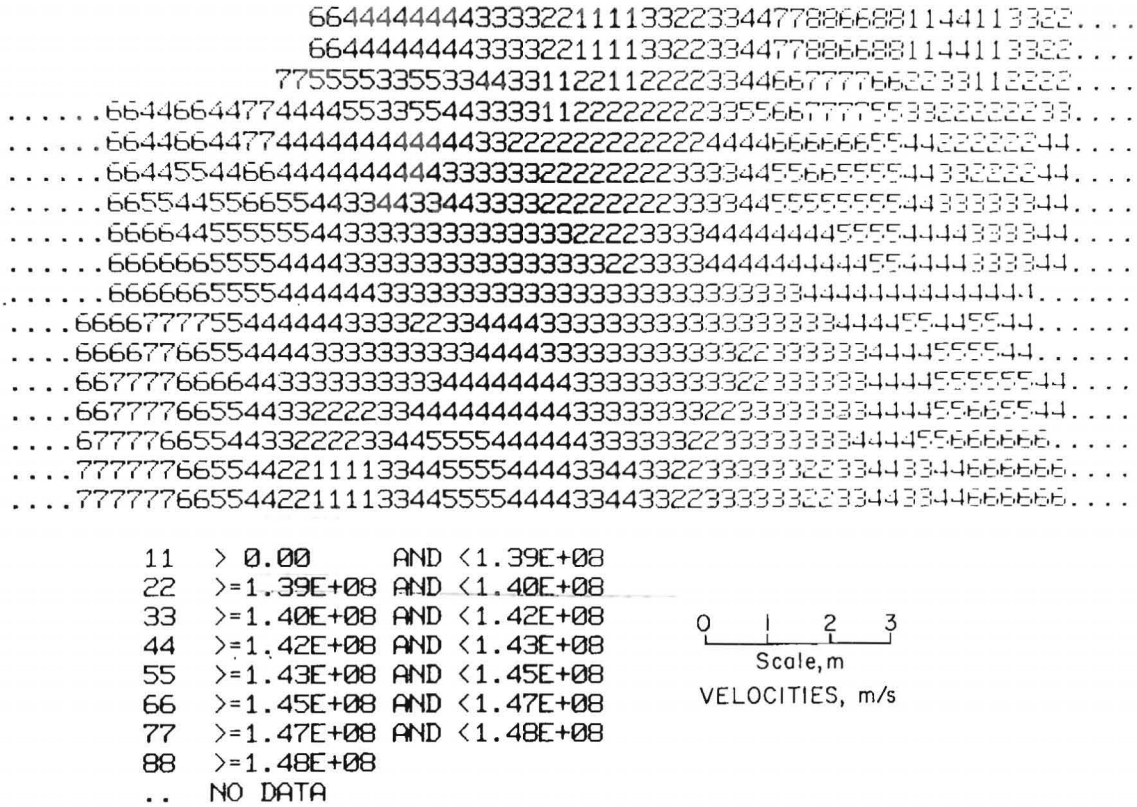


FIGURE 22.—Line printer tomographic plot of velocity cells from short-pulse data. Two horizontal characters represent one cell.

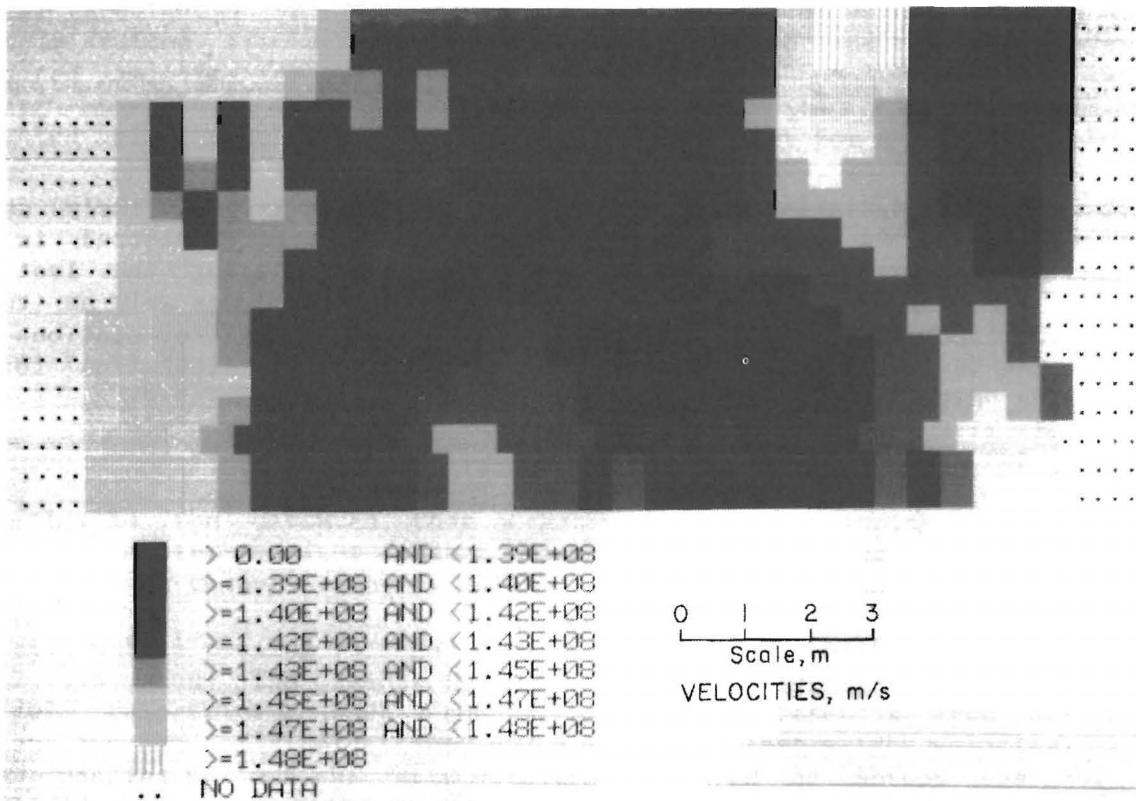


FIGURE 23.—Gray scale tomographic plot of short-pulse data.

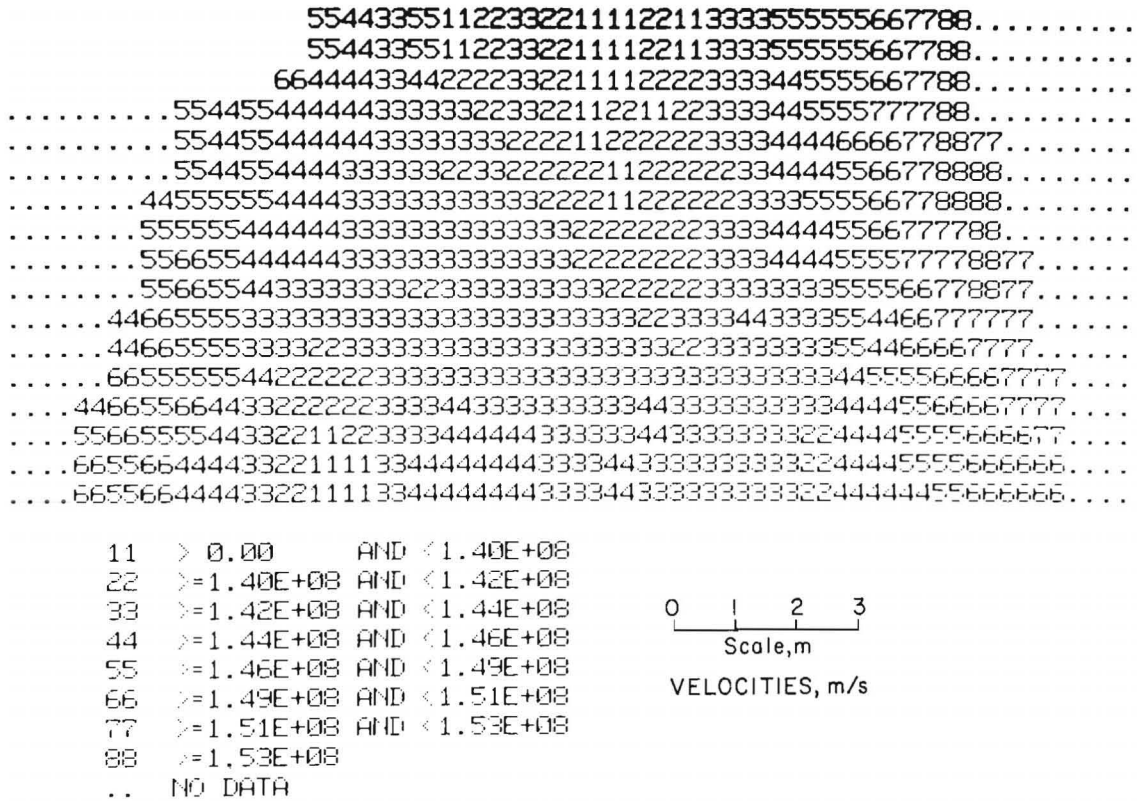


FIGURE 24.—Line printer tomographic plot of velocity cells from synthetic-pulse data. Two horizontal characters represent one cell.

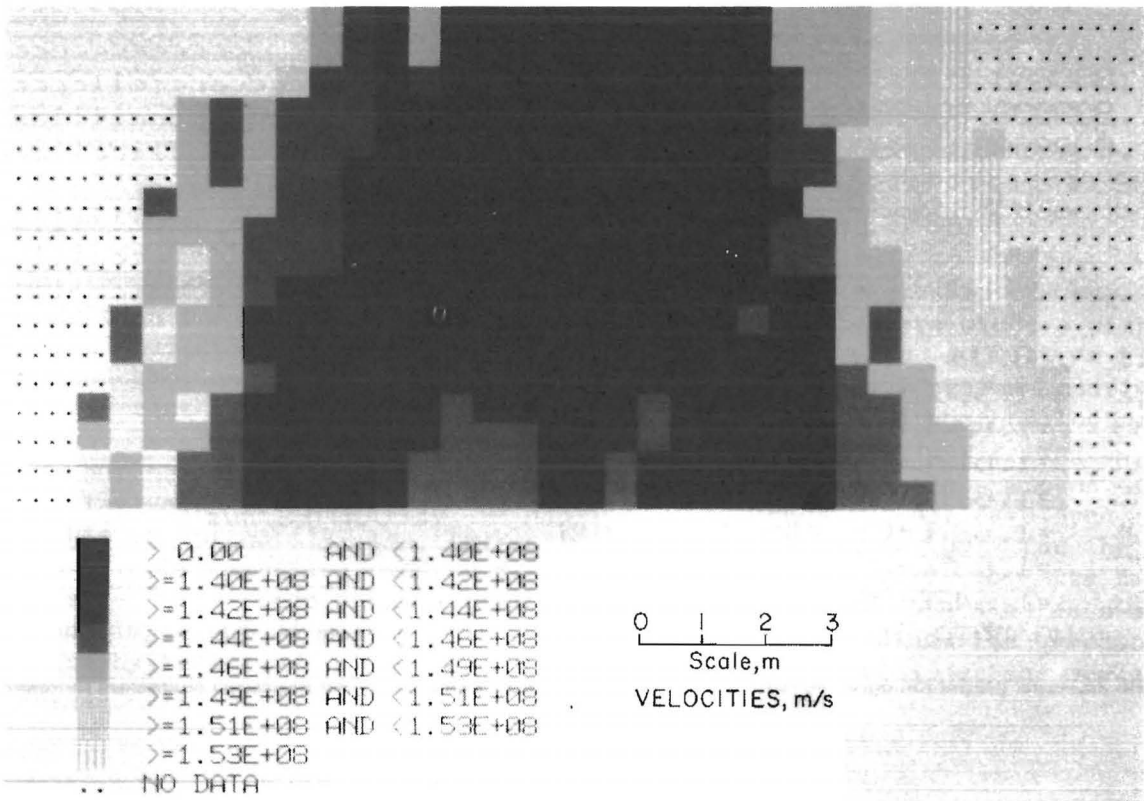


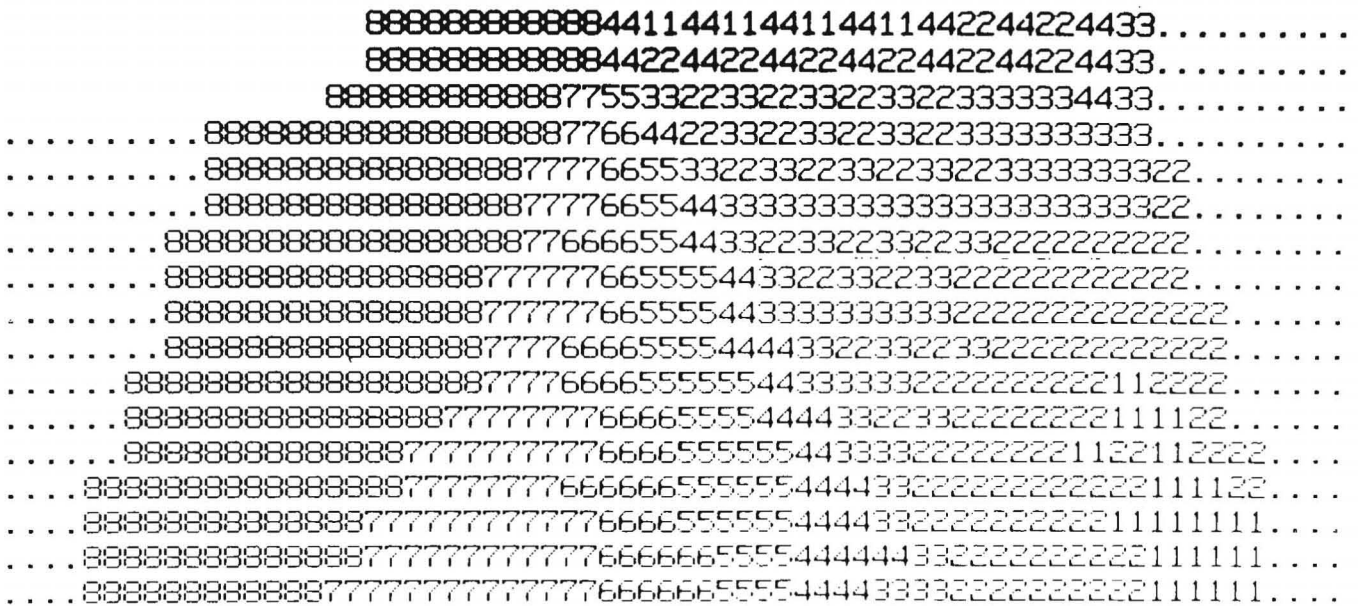
FIGURE 25.—Gray scale tomographic plot of synthetic-pulse data.

PHASE 3: CLAY VEIN MODEL

The interpretation of the tomographic image is not as simple or obvious as one would like. The clay vein does not appear as a band across the image. This is due mainly to the two-sided measuring procedure that was incorporated. Using computer modeling, the expected results for this clay vein were generated using the same transmitter-receiver geometries as in the field test. The results of that model are shown in figures 26 and 27. The velocities assumed for the model were based on published data (2) and were 1.65×10^8 m/s for the coal and 1.08×10^8 m/s for clay. In comparing the model to the short-pulse images (figs.

22-23), we see that the bottom right-hand corner patterns, where the vein leaves the pillar, are similar but with opposite velocities. Likewise, there are the same general type of trends for both the model and the image. This leads us to believe that the vein or its influence has shown up in the data.

The fact that the clay vein does not appear as a distinct band, even in the model, leads to the conclusion that the back projection tomography technique does not provide sufficient detail for the purpose of locating anomalous areas. This implies that more sophisticated tomography techniques should be investigated and implemented in future applications.



11 > 0.00 AND < 1.596E+08
 22 >= 1.596E+08 AND < 1.604E+08
 33 >= 1.604E+08 AND < 1.612E+08
 44 >= 1.612E+08 AND < 1.619E+08
 55 >= 1.619E+08 AND < 1.627E+08
 66 >= 1.627E+08 AND < 1.635E+08
 77 >= 1.635E+08 AND < 1.642E+08
 88 >= 1.642E+08
 .. NO DATA

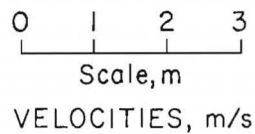


FIGURE 26.—Line printer tomographic plot of velocity cells from clay vein model. Two horizontal characters represent one cell.

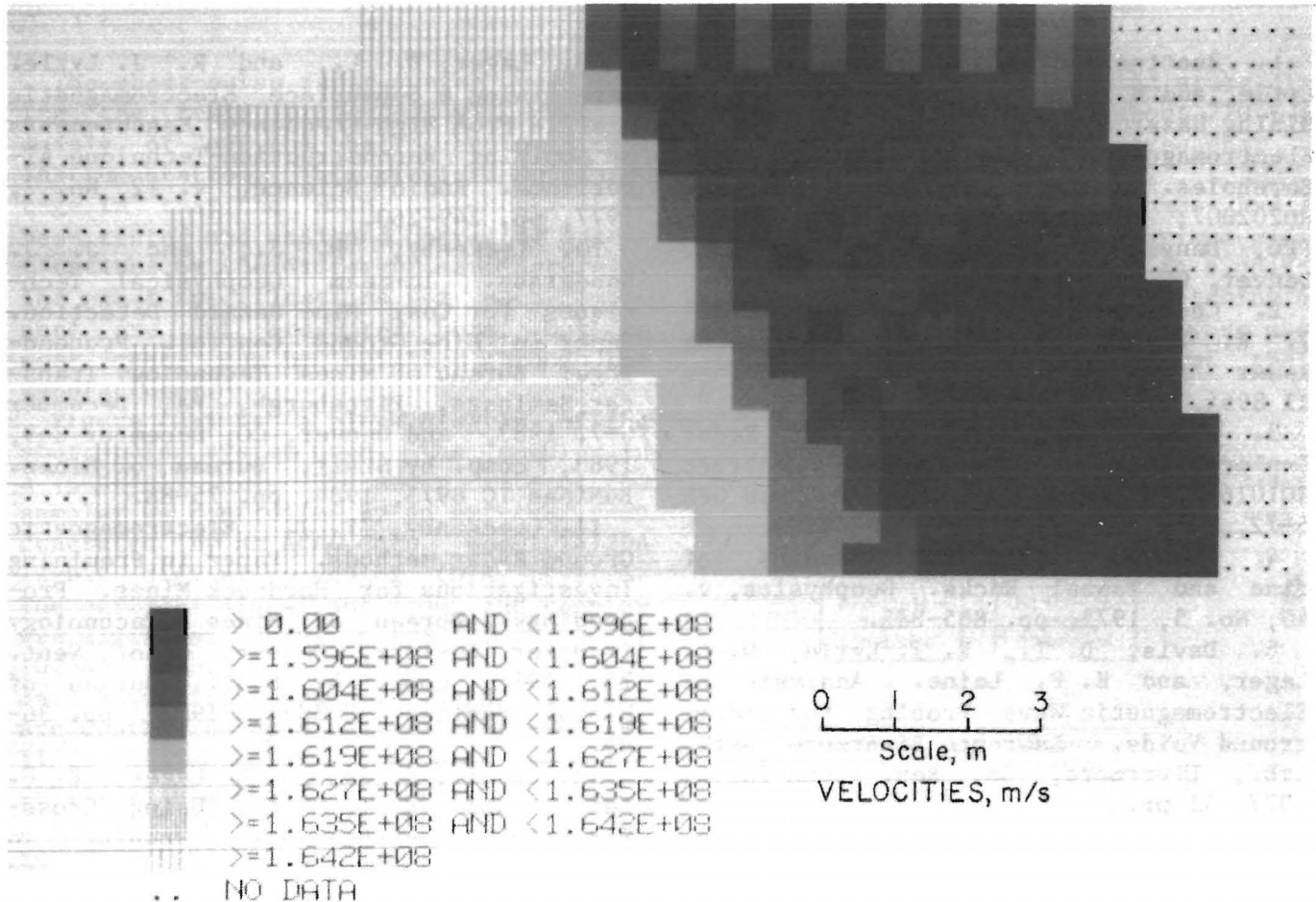


FIGURE 27.—Gray scale tomographic plot of clay vein model.

CONCLUSIONS AND RECOMMENDATIONS

In conclusion, we have determined that GPR can be used to image coal pillars and panels. The sizes and types of anomalies and hazards that can be detected are still dependent on the contrast between the electrical and other properties of the anomaly and the coal host medium. The tomography test results for the short-pulse and synthetic-pulse systems were similar, but neither has conclusively shown the clay vein of interest. The reason for this is primarily the back projection tomography technique used, and consequently a need has been established to research and implement a more sophisticated tomography technique. These preliminary studies have served to point the

direction for future research. In addition to investigating better tomography techniques, work needs to be done on understanding and integrating the amplitude data, on performing more studies with the synthetic-pulse system in both a transillumination and reflection configuration, and on devising methodologies for interpreting the tomographic images. The final conclusion is that ground radar tomography, when further developed, will prove to be a valuable tool for the mining industry, not only for its hazard detection capability but also as a means to aid in understanding the mechanical and physical properties of the media under investigation.

REFERENCES

1. Buettner, H. M., E. F. Laine, R. J. Lytle, and M. R. Portnoff. Detection of Mining Hazards and Geologic Conditions by Electromagnetic and Seismic Probing From Boreholes. Ongoing BuMines contract H0202007; for inf., contact M. M. Foss, TPO, Denver Research Center, BuMines, Denver, CO.
2. Church, R. H., W. E. Webb, and J. R. Boyle, Jr. Ground-Penetrating Radar for Strata Control. BuMines RI 8954, 1985, 16 pp.
3. Cook, J. C. A Study of Radar Exploration of Coal Beds (contract H0101620, Teledyne Geotech). BuMines OFR 5-72, 1972, 32 pp; NTIS PB 207 362.
4. _____. Radar Transparencies of Mine and Tunnel Rocks. Geophysics, v. 40, No. 5, 1975, pp. 865-885.
5. Davis, D. T., R. J. Lytle, D. L. Lager, and E. F. Laine. Analysis of Electromagnetic Wave Probing for Underground Voids. Lawrence Livermore Natl. Lab., Livermore, CA, Rep. UCRL-52214, 1977, 41 pp.
6. Ellerbruch, D. A., and J. W. Adams. Microwave Measurement of Coal Layer Thickness. U.S. Dep. Commerce, NBSIR 74-387, Sept. 1974, 29 pp.
7. Fowler, J. C., S. D. Hale, and R. T. Houck. Coal Mine Hazard Detection Using Synthetic Pulse Radar (contract H0292025, ENSCO, Inc.). BuMines OFR 79-81, 1981, 86 pp.; NTIS PB 81-224412.
8. Fowler, J. C. Coal Mine Hazard Detection Using Synthetic Radar. Ongoing BuMines contract H0212016, for inf., contact M. M. Foss, TPO, Denver Research Center, BuMines, Denver, CO.
9. Lager, D. L., and R. J. Lytle. Determining a Subsurface Electromagnetic Profile From High-Frequency Measurements by Applying Reconstruction-Technique Algorithms. Radio Science, v. 12, No. 2, 1977, pp. 249-260.
10. Leckenby, R. J., and J. J. Snodgrass. In-Seam Geophysical Techniques for Coal Mine Hazard Detection. Paper in Mine Ground Control. Proceedings: Bureau of Mines Technology Transfer Seminars, Pittsburgh, PA, December 6-7, 1983, and Denver, CO, December 8-9, 1983, comp. by Staff, Bureau of Mines. BuMines IC 8973, 1984, pp. 75-88.
11. Leckenby, R. J. Electromagnetic Ground Radar Methods. Paper in Premining Investigations for Hardrock Mines. Proceedings: Bureau of Mines Technology Transfer Seminar, Denver, Colo., Sept. 25, 1981, comp. by Staff, Bureau of Mines. BuMines IC 8891, 1982, pp. 36-45.
12. Lytle, R. J., D. L. Lager, E. F. Laine, and D. T. Davis. Using Cross-Borehole Electromagnetic Probing To Locate a Tunnel. Lawrence Livermore Natl. Lab., Livermore, CA, Rep. UCRL-52166, 1976, 41 pp.
13. Pittman, W. G., Jr., R. H. Church, W. E. Webb, and J. T. McLendon. Ground Penetrating Radar. A Review of Its Applications in the Mining Industry. BuMines IC 8964, 1984, 23 pp.
14. Skolnik, M. I. Introduction to Radar Systems. McGraw-Hill, 1962, pp. 264-265.

APPENDIX

The short-pulse radar system used during the tests presented was composed mainly of "off the shelf" equipment and instrumentation. This provided an advantage in that the main components have been tested and assigned operating specifications by the different manufacturers. The exact specifications for each component are not presented here, but in most cases can be obtained through the manufacturer.¹

Figure A-1 is a block diagram of the short-pulse system used. The sampler is a Tektronix 7S14. The sweep rate of the sampler was controlled by an external ramp generated by an ADAC Corp. model 1412DA 12-bit digital-to-analog (D/A) system. The vertical signal out from the sampler was digitized using an ADAC Corp. model 1023AD 12-bit analog-to-digital (A/D) data acquisition system. The A/D and D/A are controlled by a Digital Equipment LSI 11/23 minicomputer. The data were recorded on Digital TU58 tapes.

The external trigger for the sampler was the received signal of a dipole antenna mounted about 5 cm from the transmitting antenna. The sampler was connected to the trigger antenna and to the receiver antenna using 75- Ω coaxial cables. A VHF-UHF television 300- to 75- Ω balun was used to help match the impedance of the antennas to that of the cables. Likewise, a 75- to 50- Ω impedance transformer was used between the cables and the sampler.

¹Reference to specific products does not imply endorsement by the Bureau of Mines.

The pulser was a rapid solid state discharge device, discharging about 220 V in approximately 2.5 ns. The frequency of the system was 15 MHz.

The notched bow tie antennas had an overall length of 1 m and a maximum width of 0.5 m at the outer ends. No significance should be placed on the notching of the antennas. These antennas were used in these tests only because of their availability.

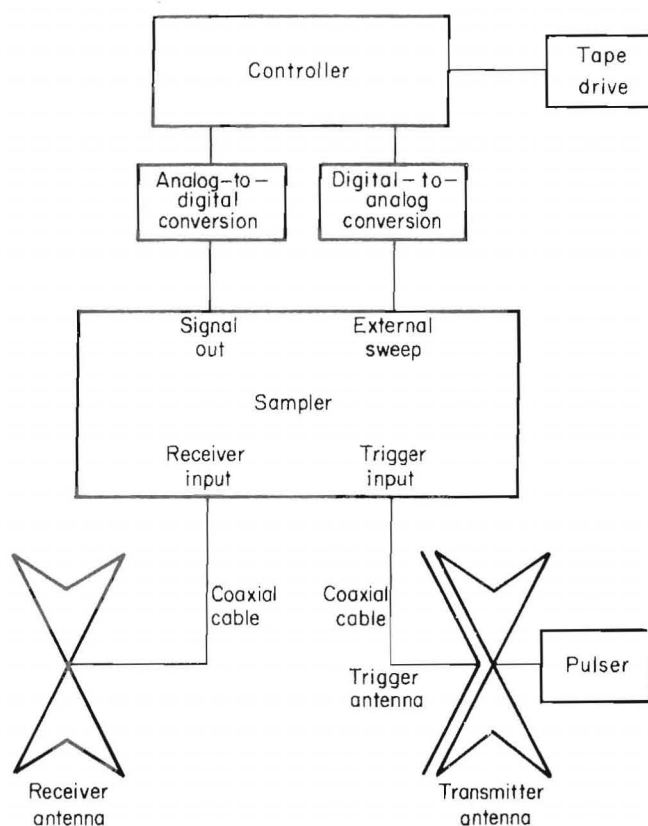


FIGURE A-1.—Block diagram of short-pulse system used during this investigation.